

## Article

# Human and Natural Activities Effects on Soil Erosion in Karst Plateau Based on QAM Model: A Case Study of Bijie City, Guizhou Province, China

Xiong Gao <sup>1,2</sup>, Pingping Yang <sup>1,2,3,\*</sup>, Zhongfa Zhou <sup>1,2</sup>, Jinqi Zhu <sup>4</sup>  and Changxin Yang <sup>1,2</sup>

- <sup>1</sup> School of Karst Science, Guizhou Normal University, Guiyang 550025, China; 222100170572@gznu.edu.cn (X.G.); fa6897@gznu.edu.cn (Z.Z.); 232100170560@gznu.edu.cn (C.Y.)  
<sup>2</sup> State Engineering Technology Institute for Karst Desertification Control, Guiyang 550025, China  
<sup>3</sup> Guizhou Karst Mountain Land Ecology and Land Use Observation and Research Station, MNR, Anshun 561301, China  
<sup>4</sup> Engineering Research Center of Watershed Carbon Neutralization, Ministry of Education, Jiangxi Institute of Ecological Civilization, School of Resources and Environment, Nanchang University, Nanchang 330031, China; zhujq@ncu.edu.cn  
\* Correspondence: pingping\_yang0320@163.com

**Abstract:** The Karst plateau region has a unique natural erosion environment and sharp human–land conflicts. This study selected Bijie City, Northwest Guizhou, as the study area. To quantitatively analyze the human and natural impacts on soil erosion in this area, this paper evaluated the anthropogenic and natural soil erosion based on the Revised Universal Soil Loss Equation (RUSLE) coupled with the Quantitative Analytical Model (QAM). The results showed the following: (1) the total soil erosion modulus in the study area showed an increasing trend: 37.86 t/(ha·a) in 2010, 42.12 t/(ha·a) in 2015, and 48.67 t/(ha·a) in 2020; (2) human activities reduced soil erosion, with an anthropogenic soil erosion modulus of −13.79 t/(ha·a) in 2015 and −17.36 t/(ha·a) in 2020, indicating that human activities, such as projects of returning farmland to forests and rocky desertification control, played a key role in decreasing soil erosion in the study area.; and (3) the percentage of the area of soil erosion deterioration dominated by natural factors (AGN) is gradually decreasing, 89.47% in 2015 and 81.85% in 2020; the percentage of the area of soil erosion deterioration dominated by human activities (AGH) is increasing from 6.17% in 2015 to 13.80% in 2020; and the percentage of the area of soil erosion mitigation caused by human activities (ALH) and the area of soil erosion not affected by natural and human activities (NNH) showed no significant change. This result suggests more attention should be paid to the area of AGH to control soil erosion. This study analyzed the roles of natural factors as well as human activities in the Karst plateau, enriched the application scope of the QAM, and provided new ideas for theoretical research in this field.

**Keywords:** Revision of the Generalized Soil Loss Equation (RUSLE); Quantitative Analytical Model (QAM); Karst plateau; anthropogenic soil erosion; Bijie City



**Citation:** Gao, X.; Yang, P.; Zhou, Z.; Zhu, J.; Yang, C. Human and Natural Activities Effects on Soil Erosion in Karst Plateau Based on QAM Model: A Case Study of Bijie City, Guizhou Province, China. *Land* **2024**, *13*, 1841. <https://doi.org/10.3390/land13111841>

Academic Editor: Nick B. Comerford

Received: 28 September 2024

Revised: 25 October 2024

Accepted: 1 November 2024

Published: 5 November 2024



**Copyright:** © 2024 by the authors. Licensee MDPI, Basel, Switzerland. This article is an open access article distributed under the terms and conditions of the Creative Commons Attribution (CC BY) license (<https://creativecommons.org/licenses/by/4.0/>).

## 1. Introduction

Soil erosion is one of the most serious environmental and public health problems [1], which leads to a decrease in the productivity of arable land and the pollution of surrounding waters such as rivers and lakes [2]. Soil erosion is the result of a combination of natural processes and human activities [3]. In the Universal Soil Loss Equation (USLE), the influencing factors of soil erosion are categorized as rainfall, soil erosion resistance, topography, vegetation cover, and soil and water conservation measures. Among the above factors, soil erosion resistance and topography are difficult to change in a short period and are non-significantly affected by natural and human activities. Rainfall is mostly governed by natural processes and less influenced by human activity. Rainfall is one of the main factors driving soil erosion, as numerous studies have demonstrated [4–7]. In the middle reaches

of the Yarlung Tsangpo River, Wang et al. [8] studied soil erosion and found that the rate of soil erosion rose by 1.8% for every 1% increase in precipitation.

The vegetation is affected by both natural processes and human activity. Moreover, soil erosion is sharply influenced by vegetation [2]. Generally, vegetation reduces soil erosion, due to the following: (1) vegetation canopies and dead leaves retain rainfall [2,9]; (2) the branches and trunks of vegetation retard surface runoff velocity [10]; and (3) the root system of vegetation can fix the soil and increase the soil shear resistance [2,11–13]. Zhang et al. [14] found that vegetation has the greatest effect on the soil erosion modulus when the vegetation cover is less than 35%. Furthermore, the effect of vegetation on the erosion modulus decreases sharply when the vegetation cover is greater than 35%.

The soil and water conservation measures are mainly affected by human activities, by way of changing land use patterns. Soil properties are influenced by land use practices [15,16]. Particularly, the increasing population results in the transforming of land use patterns and farmer management [17], which can further affect soil erosion [18]. Gocić et al. [19] demonstrated in the Jablanica River Basin, Serbia, that land use changes, such as cropland abandonment, have significantly impacted soil erosion. Zhao et al. [20] found that the soil erosion rate of grass-covered land classes was 1–3 orders of magnitude lower than that of agricultural land. Obiahu et al. [21] showed that land use and land cover change are the major causes of soil erosion in Nigeria; Borrelli et al. [22] assessed the global soil erosion rate in 2001 and 2012, and found that soil erosion on cropland was 7 times higher than that of natural forests and concluded that the acceleration of soil erosion is because of land use changing.

Human activities have both negative and positive effects on soil erosion. In recent years, with the advancement of environmental awareness in China, many soil and water erosion control measures have been carried out, which are mainly based on biological measures and supplemented by engineering measures [23]. China's soil and water conservation measures in the upper reaches of the Yangtze River have reduced the area of water erosion from 37.2–63.2% to 23.5–38.1% [23]. Han et al. [24] evaluated the soil erosion modulus of the Baocheng Gou watershed of the Loess Plateau by using the USLE, to assess the impact of the gully land consolidation project, which led to a 18.6% reduction in soil erosion in the area. Jin et al. [5] demonstrated that soil erosion on the Loess Plateau has been on a downward trend because of the change in surface conditions such as vegetation cover and soil and water conservation measures, which have contributed 119% to the erosion reduction.

The karst region of southwestern China exhibits a distinctive natural erosion environment, including the exposure of bedrock surfaces, the presence of shallow soil layers, and the occurrence of dual (surface–subsurface) erosion processes [25]. The mechanisms of soil erosion in this region diverge from those observed in non-karst areas. Furthermore, the region is one of the areas in China where the population living in poverty is concentrated, and the intense human–land conflict has led to more intensive development activities [26]. This further exacerbates the occurrence of local rock desertification and causes soil erosion [27,28], especially in the Karst plateau area of northwest Guizhou, where the population is large and has a widespread typical karst landscape. Since 1999, a number of karst ecological restoration projects have been implemented in Southwest China, including the “grain-for-green program”, “natural forest protection project”, and “public welfare forest protection”. Qiao et al. [29] demonstrated those projects promoted the recovery of local vegetation and exerted a positive effect on soil and water conservation [30].

Recent studies indicated that rainfall can exacerbate soil erosion. Yang et al. [31] proposed that the quantity, frequency, and intensity of precipitation can influence rainfall erosivity, which, in turn, affects soil erosion. The detrimental effects of climate change on soil erosion resulting from global warming cannot be overlooked. Peng et al. [32] observed a significant increase in precipitation from 2000–2015 in Guizhou province, with climate contributing to a 71% change in soil retention. Zhu et al. [33] examined the rainfall patterns in the Karst region of southern China between 1960 and 2017 and indicated that the annual rainfall erosivity in the region has been on the rise. Hence, there is a complex interaction between natural and anthropogenic influences on soil erosion in karst areas. It is necessary

to quantify the role of local anthropogenic factors on soil erosion, focusing on the role of human activities such as ecological restoration projects on soil erosion in the karst area.

Currently, few works of research have paid attention on quantitatively analyzing soil erosion from human activities and the natural environment in the Karst plateau region. The quantification of human and natural soil erosion in this region can facilitate the improvement in the soil erosion mechanism and provide theoretical support for local soil and water conservation decision-makers. To address the above issues, we studied the soil erosion of Bijie City in northwest Guizhou, China, where the area of rocky desertification is 598,400 ha. All types of karst rocky desertification can be found here [34]. Since 2011, all districts and counties have been included in the national key counties for the comprehensive management of rocky desertification, with the implementation of the comprehensive management of rocky desertification in these areas. Additionally, Bijie is the most populous city in Guizhou Province and is characterized by a significant human–land conflict.

This study introduces the Quantitative Assessment Model (QAM, [3]) based on the Revised Universal Soil Erosion Equation (RUSLE) to evaluate the soil erosion in Bijie City. The objective of this study aims to accomplish the following: (1) the quantification of the natural and anthropogenic soil erosion and analysis of the structure of the anthropogenic and natural soil erosion in Bijie; (2) the identification of the type of soil erosion; and (3) the evaluation of the effectiveness of the recent implementation of projects such as returning farmland to forests and soil conservation management. The findings of this study may provide novel insights and methodologies for the investigation of soil erosion and soil and water conservation in karst regions.

## 2. Study Area and Methods

### 2.1. Study Area

Bijie City is situated in the northwestern part of Guizhou Province in southwestern China, with a total area of 26,900 km<sup>2</sup> and an average elevation of 1689 m, which represents the highest average elevation area in Guizhou Province. The topography of the study area is characterized by a high elevation in the west and a low elevation in the east. Karst landforms are widely distributed. The eastern part exhibits peak forests, valleys, peaks, gentle hills, and depressions. The central part displays peaks and troughs. The western part is characterized by the development of plateaus, gentle hills, and basins. Sedimentary rocks are the dominant rock type observed in the outcrops, with exposed limestone and dolomite accounting for 66.5% of the total area. The study area is situated within a humid subtropical monsoon climate zone, characterized by abundant rainfall, with an average annual precipitation of 1200 mm and an average annual evaporation of more than 1000 mm. The vertical climate change is particularly evident due to the large difference in altitude. The soil is dominated by yellow and yellow-brown loam, with the majority of the vegetation comprising secondary evergreen broad-leaved mixed forest. We found that 4.61% of the territory belongs to the North Pearl River Basin, while 95.39% belongs to the Yangtze River Basin. There are 193 rivers longer than 10 km, which flow into the Wujiang River, Chishui River, Beipanjiang River, and Jinshajiang River. The density of the river network is 0.5 km/km<sup>2</sup>. By the end of 2020, the forest area of the study area is 161,067,700 hm<sup>2</sup>, with a coverage of 60%. We found that 11 nature reserves have been established in this area (Figure 1), with a total area of 53,932.4 hm<sup>2</sup>, accounting for 2.01% of the total area.

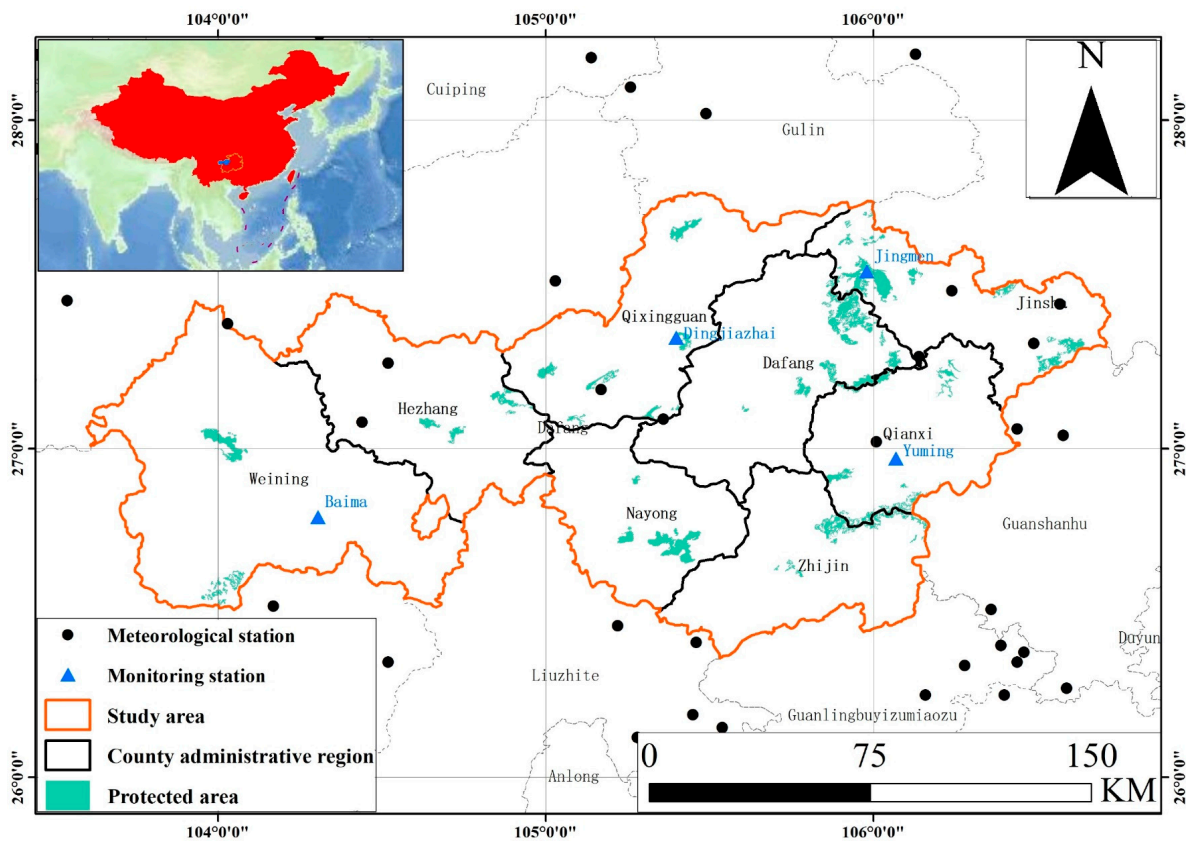


Figure 1. Study area.

2.2. Data Sources

The data employed in this study include data of climate, soil, Digital Elevation Model (DEM), Normalized Difference Vegetation Index (NDVI), land use, and rock desertification survey and protected area. The climatic data employed in this study comprise the daily value dataset of China’s surface climate data (V3.0), which encompasses daily values of barometric pressure, air temperature, precipitation, evaporation, relative humidity, and other variables at 699 meteorological stations across China since January 1951. The soil data utilized is from the World Unified Soil Database (WUSDB) 1.1. The DEM data employed is from the GDEMv3 30M dataset. The NDVI data was obtained by extracting MODIS standard products adopted from 1990 to 2022 using the Google Earth Engine platform. The 30 m land cover dataset was utilized to obtain land use data. Additionally, data from the rocky desertification survey and protected areas in Guizhou, China, were sourced from the Guizhou Forestry Bureau. The data sources are presented in Table 1.

Table 1. Data source.

Description	Name	Source
Climate data	The daily data set of China’s ground climate data V3.0	<a href="ftp://ftp.ncdc.noaa.gov/pub/data/noaa/isd-lite/">ftp://ftp.ncdc.noaa.gov/pub/data/noaa/isd-lite/</a> (accessed on 1 September 2023)
Soil data	World Unified Soil Database 1.1 (HWSD)	<a href="https://doi.org/10.12072/ncdc.westdc.db3647.2023">https://doi.org/10.12072/ncdc.westdc.db3647.2023</a>
DEM	GDEMv3 30M	<a href="https://lpdaac.usgs.gov/products/astgtmv003/">https://lpdaac.usgs.gov/products/astgtmv003/</a> (accessed on 27 September 2024)
NDVI	MODIS	<a href="https://modis.gsfc.nasa.gov/">https://modis.gsfc.nasa.gov/</a> (accessed on 1 September 2023)
Land use data	1990–2021 China 30 m Resolution Annual Land Cover Dataset and Its Dynamics	<a href="https://doi.org/10.5281/zenodo.4417810">https://doi.org/10.5281/zenodo.4417810</a>
Stony desertification survey data and protected area data	Guizhou’s Third Rocky and Forestry Survey data	Guizhou Forestry Bureau

### 2.3. Research Methods

#### 2.3.1. RUSLE Model

The RUSLE model requires less data and has excellent overall performance, making it a popular choice for soil erosion assessment and prediction studies in China. However, the simulation results of the RUSLE model in karst areas had been found to have significant errors. As a result, the study adopted the RUSLE model of Pan et al. [35] after the introduction of rock desertification factors.

$$A = (1 - \alpha) \cdot R \cdot K \cdot LS \cdot C \cdot P \quad (1)$$

where  $A$  represents soil erosion modulus, t/(ha·a);  $R$  represents rainfall erosivity factor (MJ·mm/(ha·h·a));  $K$  represents soil erodibility factor (t·ha·h/(ha·MJ·mm));  $LS$  is the topographic factor, dimensionless, and comprised of slope length ( $L$ ) and slope gradient ( $S$ );  $C$  is the vegetation cover and crop management factor, which is dimensionless and has a range of 0 to 1;  $P$  represents soil and water conservation measures factor, dimensionless; and  $\alpha$  represents the degree of rock exposure, dimensionless.

The monthly rainfall erosivity model proposed by Yu and Rosewell [36], which has been demonstrated to perform well in the southwestern region [33], was employed to calculate the factor  $R$ . The factor  $K$  was calculated using the formula proposed by Sharpley and Williams [37], which considers the carbon content of the topsoil.

The method proposed by Cai et al. [38] was utilized to calculate the factor  $C$ . Factor  $LS$  was calculated using the method proposed by McCool et al. [39,40].

The factor  $P$  has been demonstrated to reduce the role of the amount and rate of soil erosion [41]. It is challenging to ascertain the factor  $P$  through the establishment of natural plots on a large scale. This study draws upon the findings of previous studies conducted in karst areas [41–43] to assign values to the factor  $P$ . The details are presented in Table 2.

**Table 2.** Soil and water conservation scores for different land types.

	Cropland	Forest	Shrub	Grassland	Water	Snow/Ice	Barren	Impervious
$P$	0.23	0.24	0.23	0.15	0	0	1	0

#### 2.3.2. QAM Model

Lang et al. [3] constructed a Quantitative Assessment Model (QAM) based on the Chinese Soil Loss Equation (CSLE) to quantify the anthropogenic soil erosion modulus in Jiangxi Province, China.

$$SEM = ASE + NaSE \quad (2)$$

where  $SEM$  is integrated soil erosion;  $ASE$  is anthropogenic soil erosion; and  $NaSE$  is natural soil erosion.

Initially, Lang et al. [3] used CSLE to calculate  $NaSE$  and  $ASE$  in Jiangxi Province. In the calculation of  $NaSE$ , the engineering measure factor and the cultivation measure factor of the CSLE model were assigned a value of 1 directly, as anthropogenic activities were not considered. It is evident that climate change and human activities interact with vegetation ecosystems [5,12]. The method was employed to establish the linear relationship between the temperature data and NDVI data of the protected area where no human activities are affected. The temperature data were employed to deduce NDVI and the vegetation cover factor  $C$  with no human activities was calculated. Consequently, the  $SEM$  and  $NaSE$  were obtained, and then the  $ASE$  was calculated by  $SEM$  subtracting  $NaSE$ . QAM model provides a new direction for the calculation of anthropogenic soil erosion, but the setting of the engineering measure factor and the cultivation measure factor is not reasonable enough. The details can be seen in Section “Land Cover Background”.

Afterward, Lang et al. [3] constructed a contribution rate (CR) calculation table (Table 3) to determine the dominant factors of soil erosion. Six types of soil erosion were classified, i.e., exacerbation dominated by natural factors (AGN), exacerbation dominated by human

activities (AGH), mitigation dominated by human activities (ALH), exacerbation dominated by both natural factors and human activities (AGC), exacerbation led by natural factors (AGN), and not influenced by natural factors and human activities (NNH).

**Table 3.** CR calculation table.

Influencing Factor		Contribution Rate %		Effect Factor		
NF	HA	NF	HA	EC	DF	EFFECT
<i>NaSE</i> > 0	<i>ASE</i> > 0	$CRN = NaSE / SEM \times 100$	$CRH = ASE / SEM \times 100$	<i>CRN</i> > <i>CRH</i> <i>CRN</i> < <i>CRH</i> <i>CRN</i> = <i>CRH</i>	<i>NF</i> <i>HA</i> <i>HA&amp;NF</i>	aggregate aggregate equivalent
	<i>ASE</i> = 0	<i>CRN</i> = 100	<i>CRH</i> = 0	<i>CRN</i> > <i>CRH</i>	<i>NF</i>	aggregate
	<i>ASE</i> < 0	$CRN = (1 - CRH) \times 100$	$CRH = ASE / (NaSE +  ASE ) \times 100$	<i>CRN</i> > 1	<i>NF</i>	aggregate
<i>NaSE</i> = 0	<i>ASE</i> > 0	<i>CRN</i> = 0	<i>CRH</i> = 100	<i>CRN</i> < <i>CRH</i>	<i>HA</i>	aggregate
	<i>ASE</i> = 0	<i>CRN</i> = 100	<i>CRH</i> = -100	<i>CRN</i> =   <i>CRH</i>	<i>HA</i>	alleviation
	<i>ASE</i> < 0	<i>CRN</i> = 0	<i>CRH</i> = 0	<i>CRN</i> = <i>CRH</i>	-	unaffected

Notes: NF is the Natural Factor; HA is Human Activity; EC is the Evaluation Condition; DF is the Dominant Factor; and CRN is the Contribution Rate of the Natural Factor. The value of CRN is in the range of 0–200%; CRH is the Contribution Rate of Human Activity, CRH is in the range of -100%–100%; and CRH + CRN = 100%.

### Correlation Analysis of NDVI and Temperature

Previous studies [5,44] have demonstrated a strong correlation between vegetation cover and climate change in Guizhou. In this study, data from meteorological stations in and near Bijie City were used to obtain the monthly mean air temperature by interpolation. The maximum monthly NDVI data were calculated using MODIS data. The correlation coefficient between the monthly mean air temperature and the monthly NDVI in the protected area was calculated. As shown in Table 4, the highest correlation coefficient in 2015 years was 0.68 in April, and the highest correlation coefficient in 2020 years was 0.75 in October. To avoid the error of NDVI values caused by seasonal changes, all regression analyses were carried out using the month of April, which exhibited the highest correlation coefficients.

**Table 4.** NDVI and temperature correlation coefficients.

	Jan	Feb	Mar	Apr	May	Jun	Jul	Aug	Sept	Oct	Nov	Dec
2015	-0.37	0.54 **	0.48	0.68 **	0.28	-0.29	0.31 **	0.10	-0.39	0.36	0.36 **	-0.15
2020	-0.37	0.10	0.61 **	0.71 **	0.59 **	0.25	0.39	-0.05	-0.27	0.75 **	-0.52	-0.52

Note: \*\* represents significance at the 0.01 level.

### Land Cover Background

In the CSLE model, Lang et al. [3] assumed a value of 1 for the engineering measure factor and the cultivation measure factor to calculate Nase. This method does not take into account the land cover background, which may lead to the NaSE overvalued. In this study, when calculating NaSE, P was assigned based on the land use background, so the calculation results are more in line with the actual situation.

Figure 2 shows the flow chart of the study. Firstly, the soil erosion modulus (SEM) for 2010, 2015, and 2020 were calculated. Secondly, the P was calculated using the 2010 data as the land cover background. The fitted relationship between the NDVI and vegetation cover in the protected area was then extracted. Finally, the temperature data were used to calculate the C by referring to the whole Bijie City NDVI data. The NaSE and ASE were calculated for the years 2015 and 2020. The CR table was employed to calculate the soil erosion contribution rate and the dominant type of soil erosion.

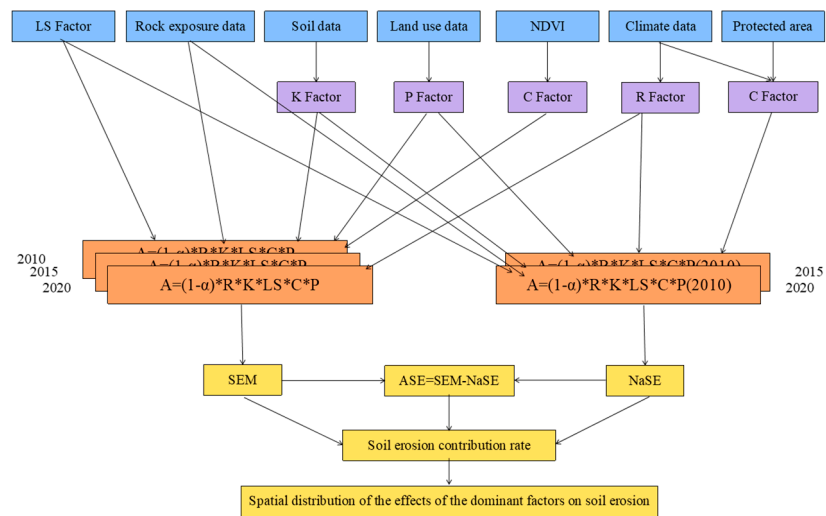


Figure 2. Flow chart.

### 2.3.3. Nash–Sutcliffe Efficiency (NSE)

Nash–Sutcliffe efficiency (NSE) is one of the main methods used to evaluate the simulation accuracy of models. In this study, NSE coefficient is used to evaluate the simulation accuracy of RUSLE.

$$NSE = 1 - \frac{\sum (y_i - \hat{y}_i)^2}{\sum (y_i - \bar{y})^2} \tag{3}$$

where  $y_i$  is the actual observation value,  $\hat{y}_i$  is the simulation result of the model, and  $\bar{y}$  is the average observation value.

## 3. Results and Analyses

The Nash efficiency coefficient (NSE) is commonly used to evaluate the effectiveness of hydrological modeling. In this study, the NSE coefficient was employed to verify the accuracy of the monitoring data from runoff plots at four monitoring stations in Bijie City; stations are shown in Figure 1. Surface runoff catchment basins were constructed below the runoff plots at each monitoring station, and the water volume and sand content of the catchment basins were measured after each rainfall. The SEM was then calculated. Due to the differing slopes, vegetation types, and coverage of the runoff plots, only the 2019 data from each monitoring station were available as a baseline. To provide a more comprehensive assessment, similar plots within 500 m of each monitoring station were selected for validation. The information for these plots is presented in Table 5. Yang [45] in the Sala Creek Demonstration Area in Bijie demonstrated that the soil subsurface leakage of runoff plots accounted for a significant proportion of the total soil erosion, ranging from 73.29% to 89.9%. These findings reflect the characteristics of surface and subsurface soil erosion in the Bijie area, with an average of 83.58%. The runoff plots at each monitoring station only observed surface soil loss; therefore, the observed results must be corrected. Figure 3 shows the corrected soil erosion and simulated soil erosion modulus of each monitoring station. The results of this correction are shown in Table 5, which indicates that the NSE is 0.76, suggesting that the RUSLE model’s simulation effect is satisfactory.

Furthermore, the working news published by the Guizhou Development and Reform Commission on the website of the Guizhou Provincial People’s Government [46] in 2011 indicated that the soil erosion modulus in Bijie, Guizhou was 33.89 t/(ha·a). The results of this study indicate that the soil erosion modulus of Bijie City was 37.86 t/(ha·a) in 2010, which is comparable to the data published by the government.

Table 5. Runoff plot information.

Monitoring Station (2019)					RUSLE (2020)				
Site	Slope °	Vegetation Type	Vegetation Cover %	Erosion Modulus t/(ha·a)		Slope °	Vegetation Type	Vegetation Cover %	Erosion Modulus t/(ha·a)
				Surface	Surface and Subsurface				
Dingjiazhai	15	Pyrus nivalis	50	13.07	79.6	15	Bush	50	46.63
Yuming	23	Natural vegetation	50	0.38	2.33	23	Arbor	50	3.53
Baima	15.8	Fallow land	23	0.48	2.91	15	Grass	39	2.675
Jingmen	15	Privet microphyll	50	1.86	0	17	Bush	50	0

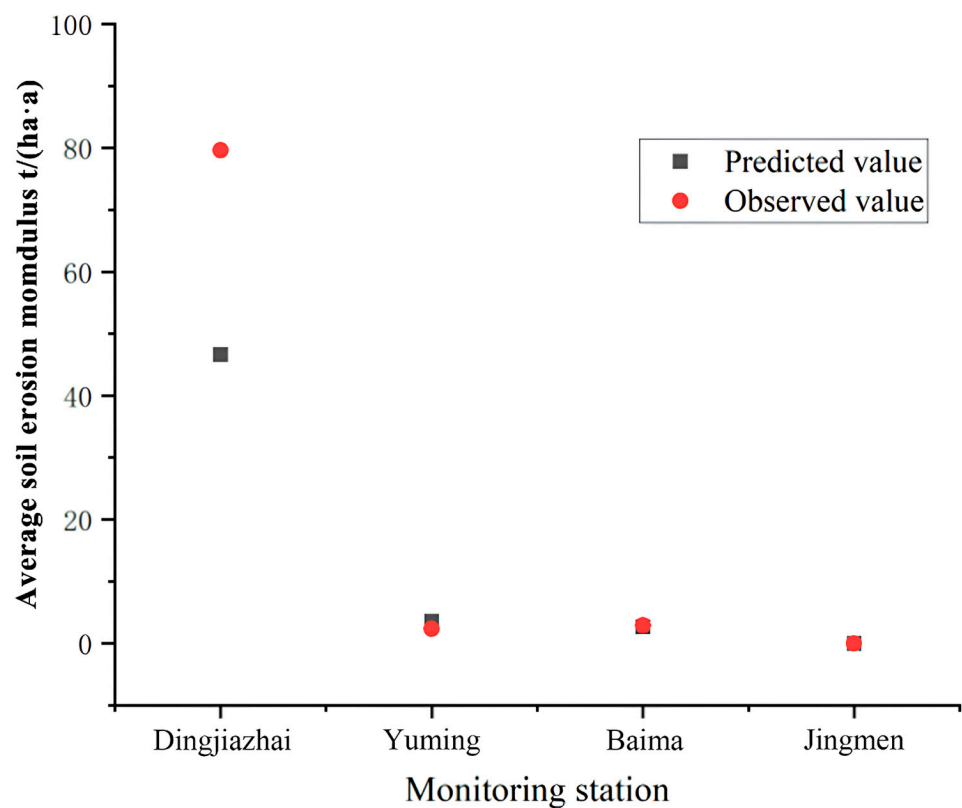


Figure 3. Observed and predicted values of each monitoring station.

### 3.1. The Total Soil Erosion Characteristics

As illustrated in Figure 4, the average SEM in the study area is on the rise, and the rising speed is accelerating. In 2015, the average erosion modulus in Bijie City increased by 11% compared with 2010. Furthermore, in 2020, it increased by 16% compared with 2015. As illustrated in Figure 5, the intensity of the SEM in the central region of Bijie City is considerably higher than that observed in the eastern and western areas. With the passage of time, the central region of soil erosion presents the trend of polarization. As shown in Table 6, This is evidenced by the increase in the area occupied by SEM < 5 t/(ha·a) and SEM > 150 t/(ha·a).

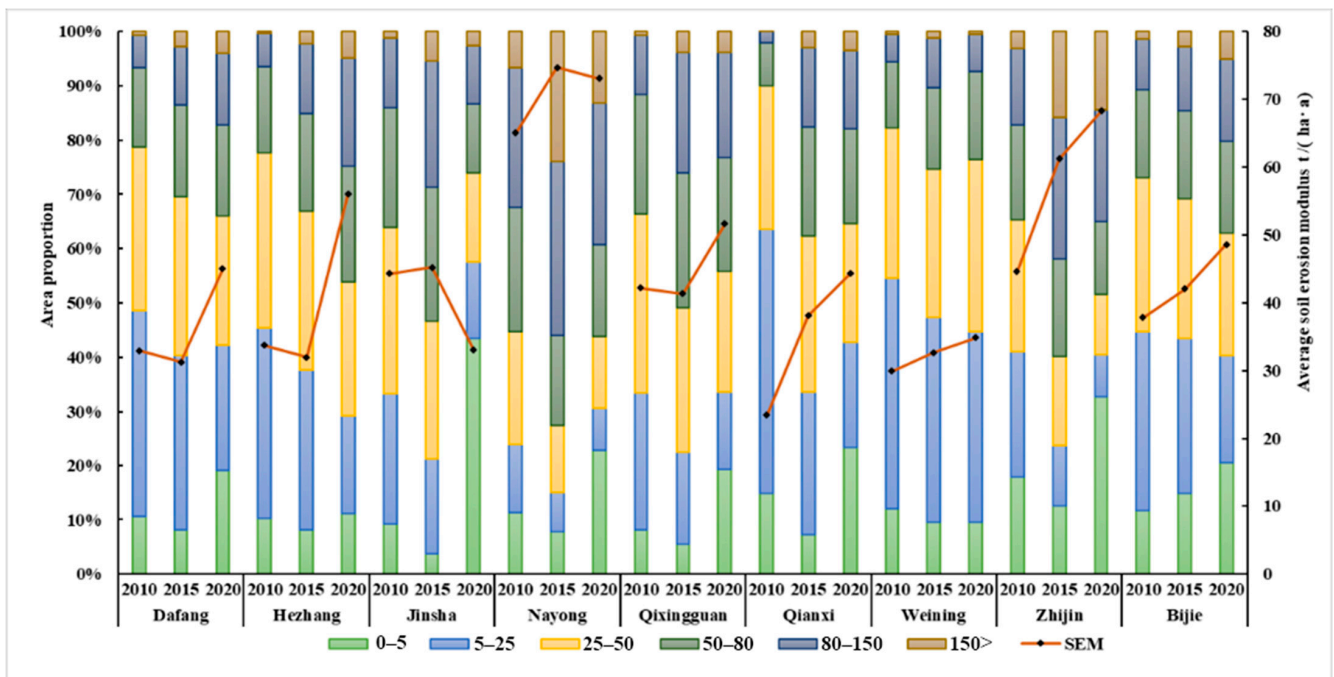


Figure 4. Average SEM in the percentage of soil erosion intensity.

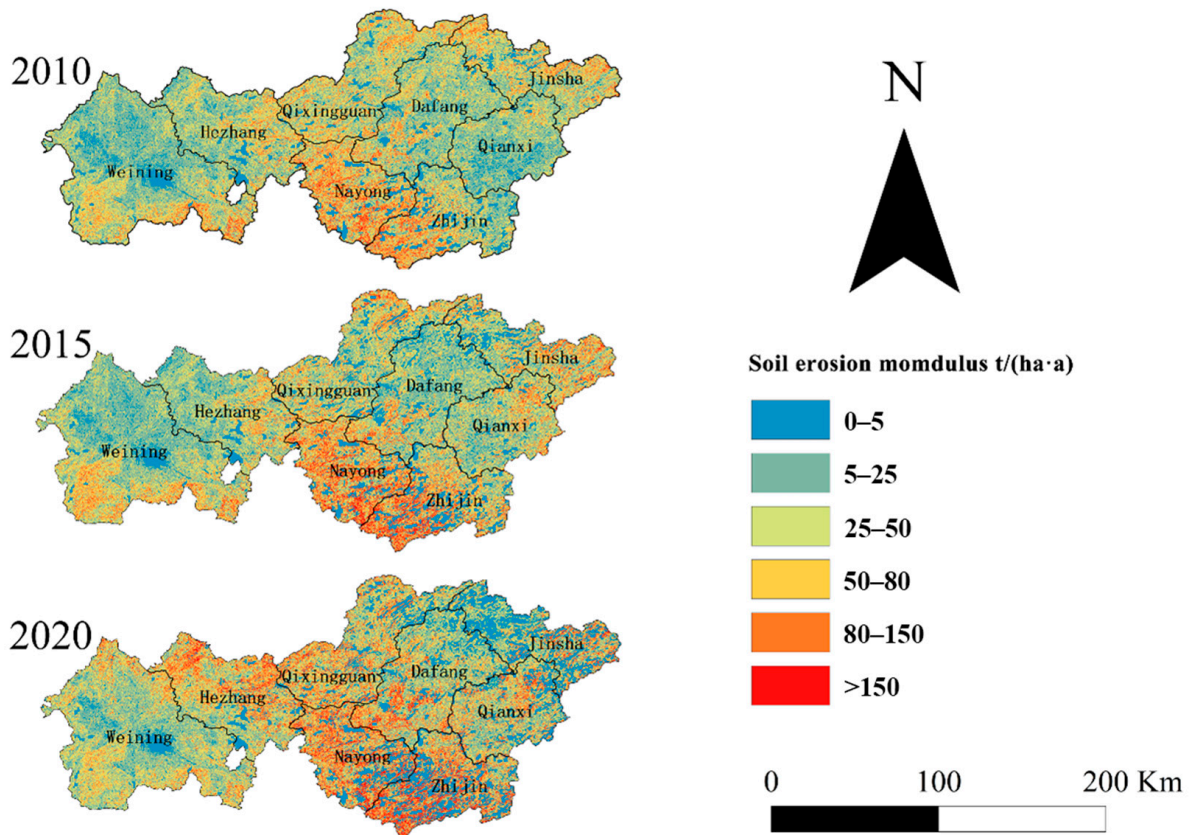


Figure 5. SEM.

**Table 6.** Percentage of natural soil erosion by class.

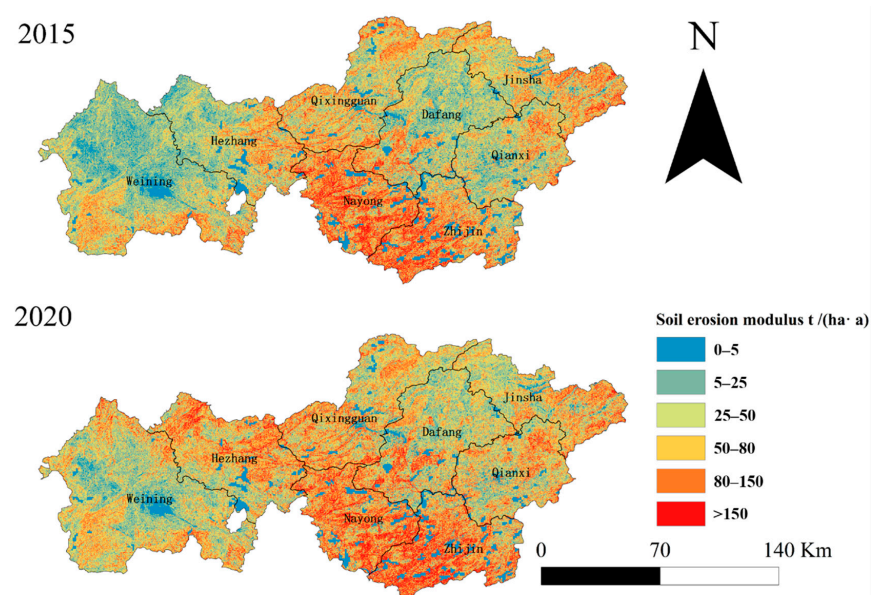
Soil Erosion Models	2015	2020
0–5	7.75%	6.39%
5–25	24.95%	18.77%
25–50	25.28%	24.05%
50–80	18.74%	20.80%
80–150	17.23%	21.37%
150>	6.05%	8.62%

In terms of counties, Nayong County exhibited the highest SEM, with a multi-year average SEM of 70.9 t/(ha·a). This was followed by Zhijin County, which exhibited a multi-year annual average SEM of 58.0 t/(ha·a). Weining County exhibited the lowest and least fluctuating SEM, with a multi-year annual average SEM of 32.5 t/(ha·a). The remaining five counties exhibited a similar range, with values ranging from 35 to 40 t/(ha·a). The SEM in Qixingguan, Hezhang, and Dafang Counties exhibited a pattern of a slight decline, followed by a pronounced increase. The most notable increase was observed in Hezhang County, where the SEM grew by 75% in 2020 in comparison to 2015. The SEM in Jinsha and Nayong Counties has declined since 2015, with Jinsha County experiencing the largest decline at 27%. In contrast, the SEM in Qianxi, Zhijin, and Weining Counties exhibited an increase, although the growth rate slowed down. The slowest growth rate was observed in Weining County.

### 3.2. Characteristics of Natural Soil Erosion Change (NaSE)

In the absence of human activities, soil erosion in Bijie City as a whole is expected to deteriorate in line with the annual average natural erosion modulus of 56 t/(ha·a) in 2015, which increased to 66 t/(ha·a). The NaSE was 0.21 t/(ha·a) in 2020, with low-intensity erosion gradually shifting to high-intensity erosion. This is evidenced by the fact that high-intensity soil erosion is mainly clustered in the central part of Bijie City.

As illustrated in Figure 6, the lowest annual average NaSE was observed in Weining County, with a value of 41.18 t/(ha·a) over the study period. Conversely, the highest annual average NaSE was observed in Zhijin and Nayong Counties, with values of 91.24 and 103.04 t/(ha·a), respectively. The annual mean NSE in Dafang and Qianxi Counties was about 52 t/(ha·a), and that in Jinsha, Qixingguan and Hezhang Counties was about 60 t/(ha·a).

**Figure 6.** NSE.

### 3.3. Characteristics of Anthropogenic Soil Erosion (ASE)

ASE is defined as the acceleration or containment of soil erosion by human activities, used to indicate the influence of human activities on soil erosion. Soil erosion is accelerated by human activities in the case of ASE >0, while soil erosion is inhibited by human activities in the case of ASE <0. A larger absolute value represents stronger human activities.

In generally, Figure 7 illustrates that human activities have reduced the soil erosion modulus in terms of the annual average soil erosion. Furthermore, the weakening value of soil erosion has been increasing year by year, with a value of  $-13.79$  in 2015 and  $-17.36$  t/(ha·a) in 2020. Figure 8 illustrates the ASE in Bijie City. In 2015, the positive effects of human activities were concentrated in the central region, while the negative effects were concentrated in the western part. In 2020, the positive effects of human activities began to be widely distributed throughout Bijie City, while the negative effects occurred mainly in the eastern hinterland.

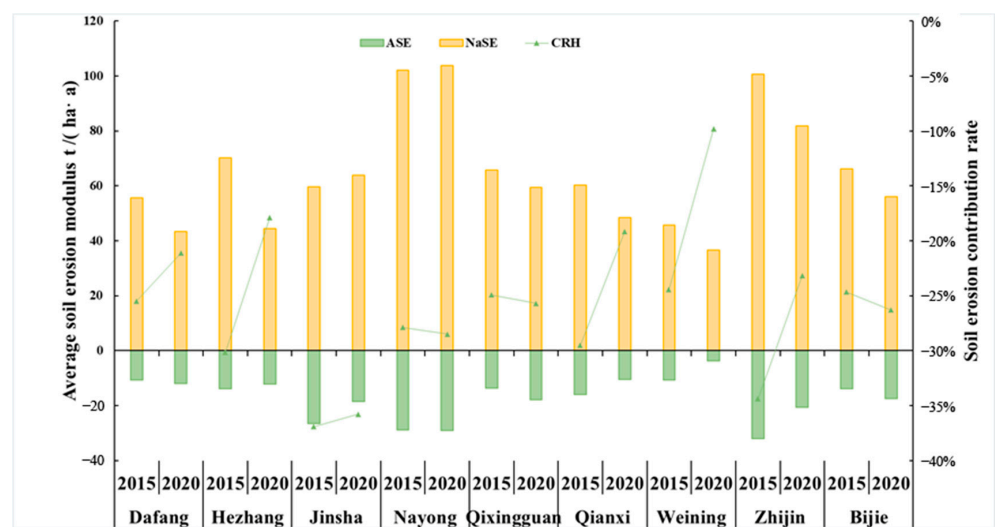


Figure 7. ASE and NSE intensity, and CRH.

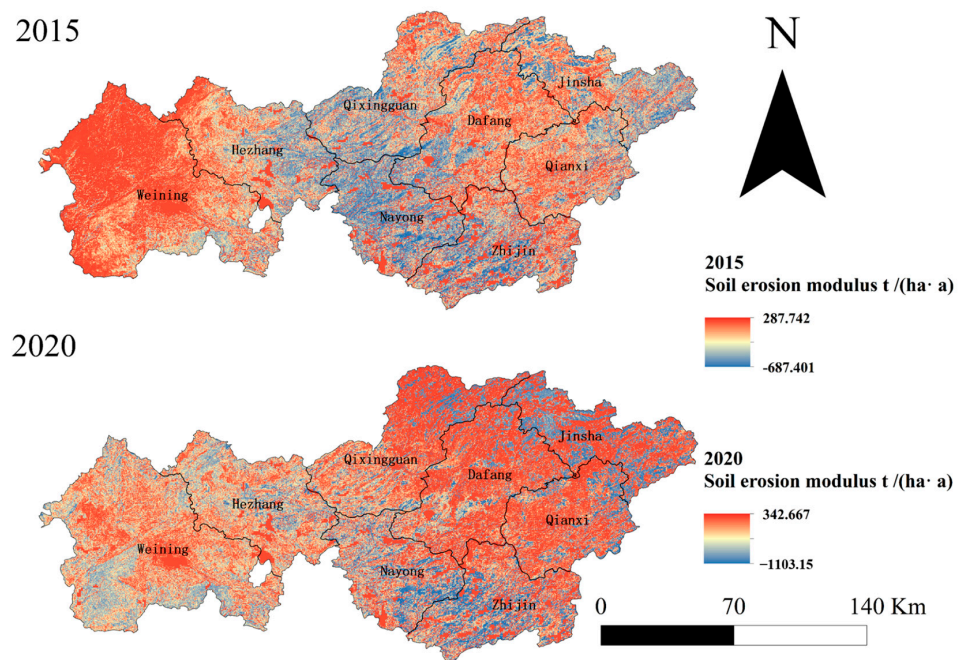


Figure 8. ASE.

The highest annual average ASE was  $-7.20 \text{ t}/(\text{ha}\cdot\text{a})$  in Weining County during the period 2010–2020. The lowest annual average ASE was found in Zhijin, Nayong, and Jinsha, with an annual average ASE of  $-26 \text{ t}/(\text{ha}\cdot\text{a})$ . The annual average ASE for the remaining counties were  $-11$ ,  $-28.99$ , and  $-22.44 \text{ t}/(\text{ha}\cdot\text{a})$ , respectively. The remaining counties exhibited a range of annual average ASE, with values between  $-11$  and  $-16 \text{ t}/(\text{ha}\cdot\text{a})$ .

### 3.4. Soil Erosion Contribution and Soil Erosion Type

Figures 9 and 10 illustrate the contribution of soil erosion in each region. It can be observed that the CRH decreased from  $-24.67\%$  in 2015 to  $-26.29\%$  in 2020. The average CRN in 2015 and 2020 was  $124.67\%$  and  $126.29\%$ , respectively.

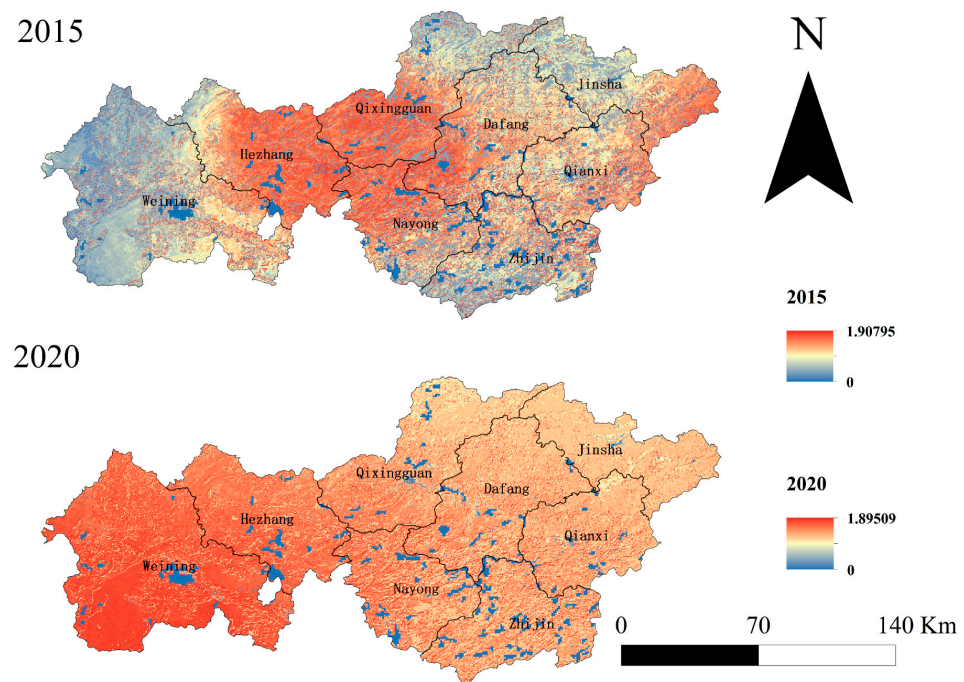


Figure 9. CRN.

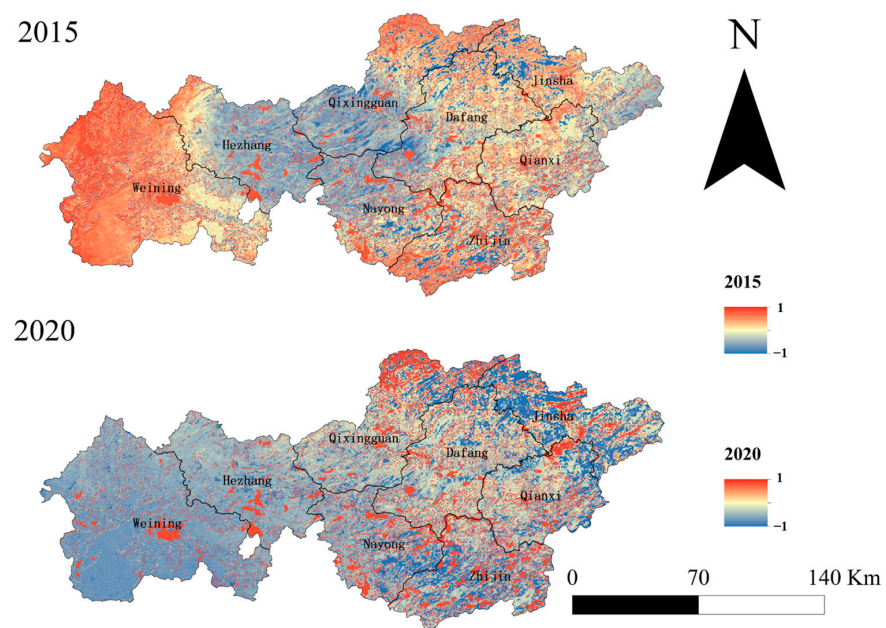


Figure 10. CRH.

As illustrated in Figure 11, four distinct types of soil erosion are observed in Bijie, namely, AGN, AGH, ALH, and NNH. AGN is the most prevalent type, occurring throughout the entirety of Bijie, followed by AGH and NNH, with AGH being particularly concentrated in the eastern region of Bijie. In contrast, ALH is the least distributed type, accounting for less than 0.01% of the total area of Bijie. As time passes, the prevalence of AGH has been on the rise. The AGN type in Bijie City has exhibited a gradual decline, with an 89.47% decrease observed in 2015 and an 81.85% decrease in 2020. Conversely, the area share of AGH has increased from 6.17% in 2015 to 13.80% in 2020. The area share of ALH and NNH has remained relatively stable.

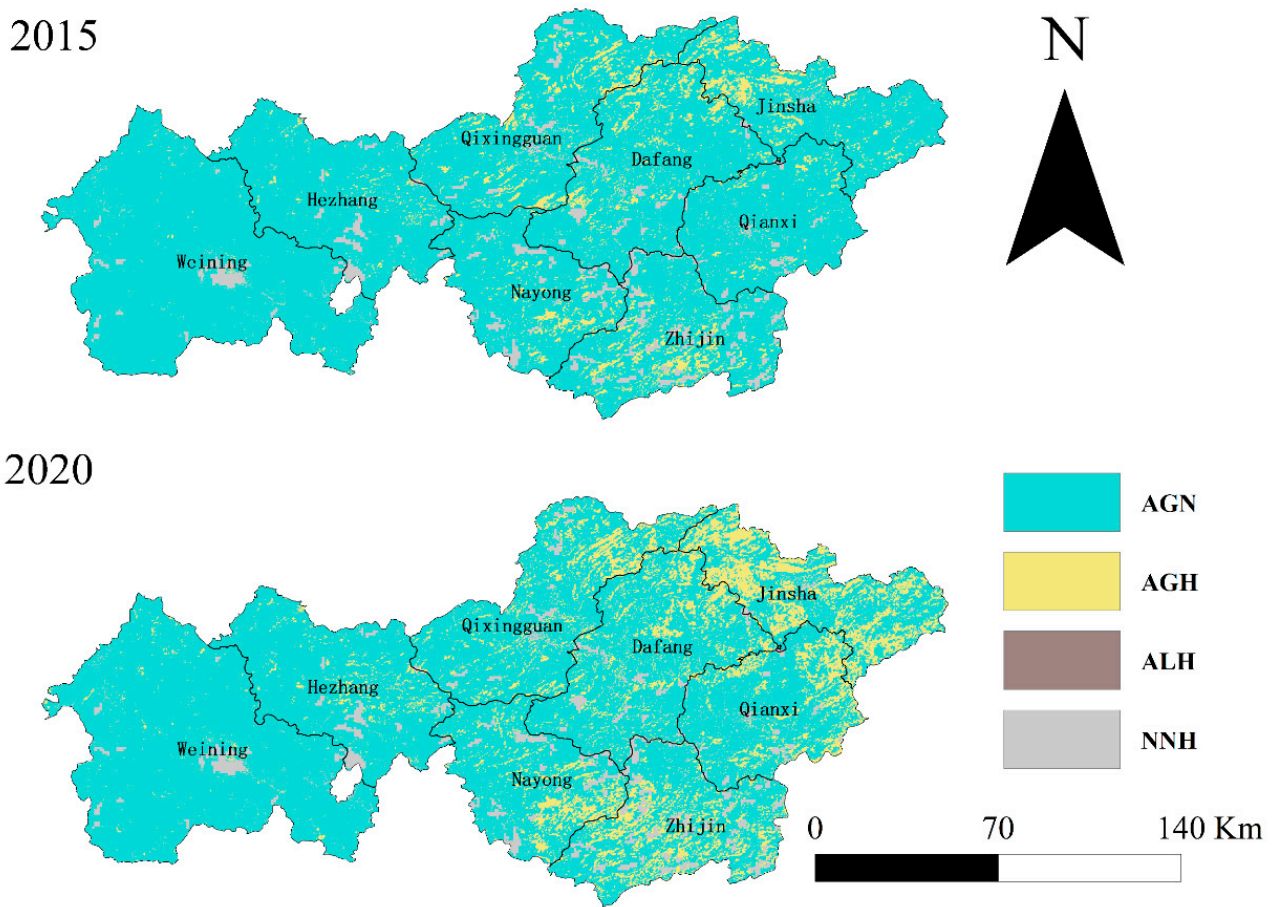
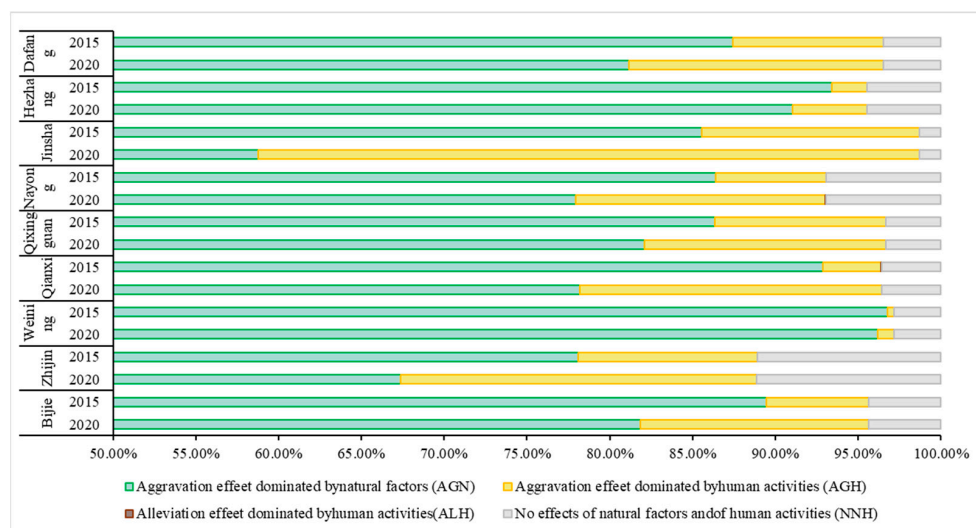


Figure 11. Spatial distribution of soil erosion types.

Figure 12 presents the percentage of soil erosion types at the county level. It can be observed that, at the county level, AGN remains the dominant soil erosion type, with a percentage exceeding 70% in all districts and counties. The highest AGN percentage is observed in Weining and Hezhang, at 96% and 92%, respectively, while the lowest AGN percentage is observed in Zhijin and Jinsha, both at around 72%. The highest percentage of AGH was observed in Jinsha, with a value of 26.53%. This was followed by Zhijin, with a value of 16.19%. The lowest percentage of AGH was observed in Hezhang and Weining, with values of 3.32% and 0.69%, respectively. The percentage of AGH in Dafang, Nayong, Qixingguan, and Qianxi was observed to be approximately 10%. The percentage of ALH in all districts and counties is less than 0.01%. The city's highest NNH ratios are observed in Zhijin and Nayong, at 11.1% and 6.95%, respectively. The exception is Jinsha, which has an ALH ratio of 1.3%. The remaining five counties have ALH ratios of approximately 3%.



**Figure 12.** Spatial distribution of leading factors of soil erosion.

A comparison of soil erosion types at the county level between 2015 and 2020 revealed a notable trend of decreasing AGN and increasing AGH. The largest region of change is in Jinsha County, where over 26.80% of the territory has changed from AGN to AGH, and, by 2020, nearly 40% of Jinsha will be of the AGH type. Next are Qianxi and Zhijin, which, in 2020, accounted for 14.70% and 10.72% of the total area transformed, and 18.23% and 21.54% of the AGH type, respectively. With only 0.6% and 2.38% of the area shifting from AGN to AGH, Weining and Hezhang have had the least amount of erosion type shift. By 2020, Weining will have 0.99% AGH type.

## 4. Discussion

### 4.1. Natural Soil Erosion

Elevation and slope are the key factors influencing soil erosion [47,48]. This study aimed to investigate the impact of natural factors on soil erosion, with a focus on elevation, slope, and vegetation type. The influence of elevation on soil erosion is primarily manifested in the relationship between elevation and rainfall, as well as the impact of human activities [48]. The topography of the Karst plateau in southwest China exhibits a pronounced elevation gradient, with the highest elevations in the west and the lowest in the east. This gradient can be used to divide the city into three distinct elevation classes [49]. The first class, which is mainly located in Weining and Hezhang Counties, is characterized by highland and mountainous terrain, with elevations ranging from 1900–2500 m. The second degree is primarily situated in Dafang County, Qixingguan District, Nayong County, and Zhijin County, characterized by mountainous terrain and elevations of 1400–1900 m. The third level is predominantly found in Jinsha County, which is a low mountainous terrain with an elevation of 1000–1400 m. As illustrated in Figure 13a, the SEM exhibits a positive correlation with elevation at lower elevations [50,51]. However, a point of variation occurs as the elevation increases, reaching between 1600 and 1800 m [51]. As shown in Figure 6, high-intensity NaSE is mainly concentrated in the second class in the central part of Karst plateau in southwest China, while the lowest grade of NaSE occurs in Weining, which is in the first class. As shown in Figure 13b, slope also provides dynamic conditions for soil erosion, with the increase in slope flow leading to the result where, the stronger the gravitational potential energy, the stronger the scouring capacity of the soil; in addition to the increase in the soil slope, this also leads to the weakening of the stability of the soil layer being more prone to be eroded by the water flow [52,53], making the soil erosion modulus higher where the slope is high. Vegetation is a significant factor influencing soil erosion, with different types of vegetation exhibiting varying degrees of influence. Wakiyama et al. [54] observed that less soil erosion occurred in coniferous forests compared to broadleaf forests

based on  $^{137}\text{Cs}$  and  $^{210}\text{Pb}$ , a finding that was also evident in this study, as illustrated in Figure 13c. Coniferous forest communities are characterized by the presence of thick moss lichens attached to the ground surface. A study by Juan et al. [55] demonstrated that the loss of sediment on slopes with moss cover was significantly reduced through simulation experiments. However, despite being coniferous forests, the soil erosion rate of coniferous forests with greater vegetation cover was found to be higher than that of coniferous forests with less vegetation cover. This phenomenon requires further investigation in subsequent studies. We suggest that the preferred choice of coniferous forests in afforestation activities in the Karst plateau area is more conducive to the prevention of soil erosion.

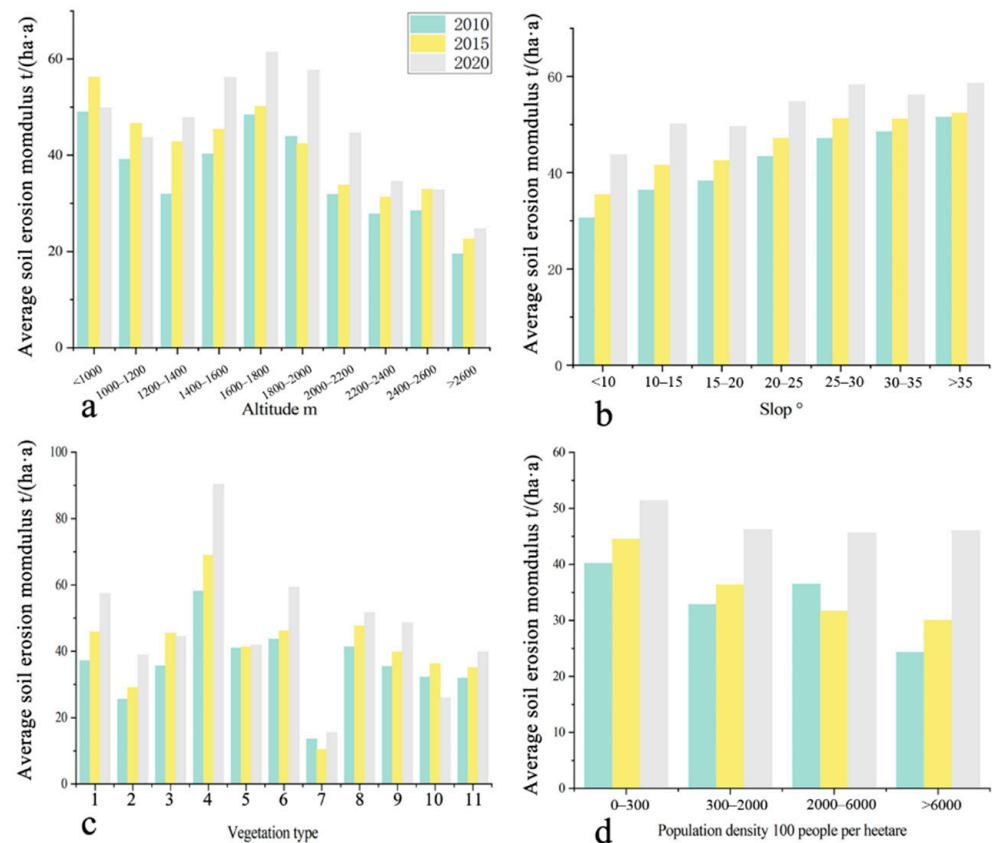


**Figure 13.** Soil erosion at different gradients of factors. (Note: (a) represents soil erosion under different altitude gradients; (b) represents soil erosion under different slope gradients; (c) represents soil erosion under different vegetation types. (d) stands for soil erosion at different population densities. In (c), 1 represents the Rainfed cropland; 2 represents the Herbaceous cover; 3 represents the Irrigated cropland; 4 represents the Open evergreen broadleaved forest; 5 represents the Closed evergreen broadleaved forest; 6 represents the Closed deciduous broadleaved forest ( $f_c > 0.4$ ); 7 represents the Open evergreen needle-leaved forest ( $0.15 < f_c < 0.4$ ); 8 represents the Closed evergreen needle-leaved forest ( $f_c > 0.4$ ); 9 represents the Shrubland; 10 represents the Evergreen shrubland; and 11 represents the Grassland.)

#### 4.2. Anthropogenic Soil Erosion

It has been demonstrated that human activities can both intensify and slow down soil erosion [56,57]. Human activities have the potential to disrupt the equilibrium of the land, which may, in turn, lead to soil erosion [58,59]. Furthermore, in the karst region, the impact of human activities on the environment may be intensified, as observed by [60,61]. Soil erosion is not solely a consequence of urban construction and crop cultivation. Indeed, a series of ecological protection measures are implemented to influence soil erosion once economic construction has reached a certain level. This is driven by the necessity to

create a better living environment and to consider future development. To mitigate the environmental impact of human activities, the local government has implemented policies and programs designed to restore the ecological balance and mitigate soil erosion. The Bijie City Environmental Bulletin indicates that soil and water conservation work was conducted annually between 2010 and 2020, with a total cumulative area of 1396.59 km<sup>2</sup> of soil. Furthermore, projects aimed at controlling soil and water erosion have been implemented on an ongoing basis. These include the return of farmland to forests and the planting of trees. As a result, the percentage of forests in the Karst plateau in southwest China has increased from 40% to 60% between 2010 and 2020. Figures 8 and 10 demonstrate a declining trend in the ASE in the Karst plateau in southwest China. This indicates that human activities have reduced the intensity of local soil erosion, both at the citywide and county levels. Figures 14 and 15 illustrate the distribution of the resident population and industries in Bijie over the past five years, with data sourced from the Guizhou Statistical Yearbook. It can be observed that Weining County has the largest population and the highest agricultural share in the city, and is one of the most densely populated counties in Guizhou Province. The high population density and agricultural share result in frequent and extensive disturbances to the land, which, in turn, leads to the highest ASE in Weining County. In contrast, in the Karst plateau region, Zhijin, Nayong and Jinsha exhibit the lowest ASE. Here, the population is the lowest and the proportion of agriculture is the lowest. The relationship between human activities and soil erosion is analyzed by dividing the population density into four gradients in terms of population density, as illustrated in Figure 13d. The expansion of urban areas increases impervious surfaces [62], a phenomenon that reduces soil sources, thereby reducing the soil erosion modulus. Furthermore, soil erosion is associated with the unequal distribution of economic costs, with densely populated areas having greater financial inputs to improve the environmental quality, which, in turn, slows down soil erosion [22]. In contrast, in suburban and even more remote areas dominated by agricultural development, especially in the Karst plateau area, due to the high topographic relief, flat land resources are very limited. Consequently, sloping plowing has become a necessity to sustain survival and development [63], which also generates more soil erosion.

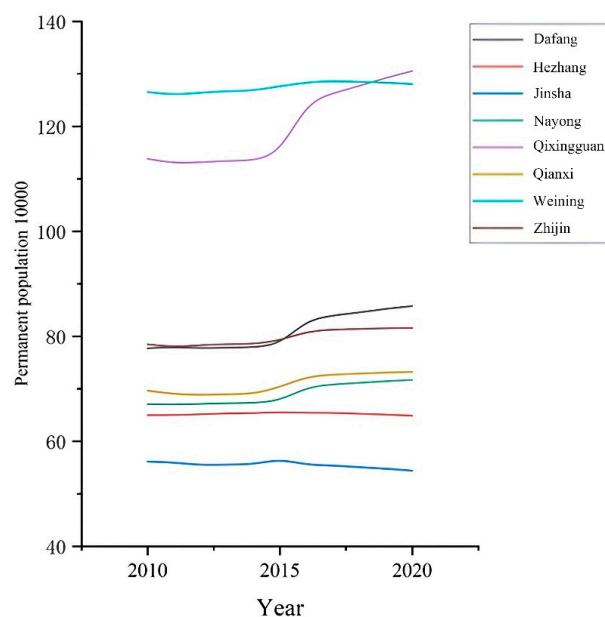


**Figure 14.** Resident population of Bijie City.

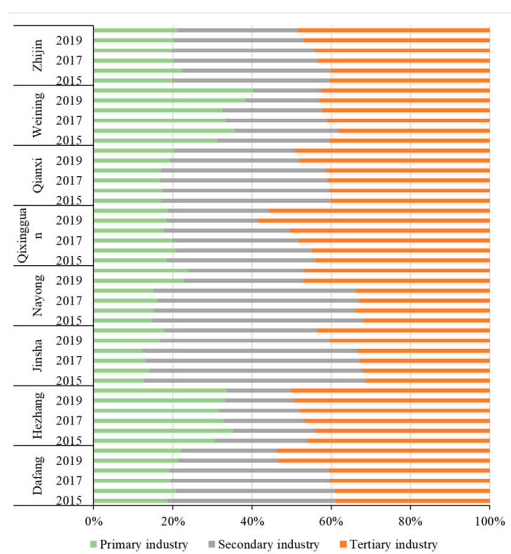


**Figure 15.** GDP of Bijie City.

#### 4.3. Total Soil Erosion

The SEM in the Karst plateau area was 37.86 t/(ha·a) in 2010, 42.12 t/(ha·a) in 2015, and 48.67 t/(ha·a) in 2020. The SEM in the Karst plateau area demonstrated an overall increasing trend, with a gradual acceleration in the growth rate. This trend aligns with the findings of the study by Zhang [51] in the Karst region of southwest China, as illustrated in Figure 16a. Among the many factors in the RUSLE model, only factors R, C, and P change with time [64]. The R is influenced by climatic conditions and reflects the relationship between rainfall and soil erosion. As economies develop, the C and P are increasingly affected by human activities. The C has a negative correlation with vegetation cover, while the P reflects the ratio of soil loss after taking certain soil and water conservation measures to the amount of soil loss when no measures are taken. Figure 16b illustrates the temporal trends of the R, C, and P factors, which are susceptible to change with time. Guizhou has long implemented the policy of returning farmland to forests and has carried out rocky desertification control projects since 2011 [65]. These policies have led to a year-on-year increase in vegetation cover in Guizhou in recent years [66,67]. The trend of NDVI values in the Southwest Karst region in recent years is illustrated in Figure 16c. It can be observed that the vegetation, which has been rising year on year, has the effect of slowing down soil erosion to a significant extent. The decreasing trend of both the C and P is related to these policies. The factors of C and P are both decreasing, but the SEM continues to rise, which should be taken seriously. In the context of global climate, the annual rainfall in China is increasing year by year, and [68] showed that the annual rainfall erosivity is generally increasing, which makes soil erosion more likely, and Lian et al. [69] and Zhu et al. [33] found a similar trend in the karst region; see Figure 16d. The continuous increase in rainfall erosivity masks the effectiveness of soil erosion control through ecological restoration, returning farmland to forests, rocky desertification management, etc. The reason for the increase in the soil erosion modulus in the Karst plateau area is mainly due to the continuous increase in rainfall erosivity.

As can be seen in Figure 16, of the many changing factors, only the R factor is increasing from year to year, while the others are decreasing. It can be seen that the increase in the area of SEM < 5 t/(ha·a) is due to the improvement brought about by human activities such as afforestation. However, although most factors are decreasing, factors such as K and LS remain constant and continue to provide conditions for soil erosion to occur. Especially in areas where it is difficult to carry out measures such as afforestation, their C and P have not changed much. The increase in the erosive power of rainfall, on the other hand, contributes greatly to the occurrence of soil erosion in these areas.

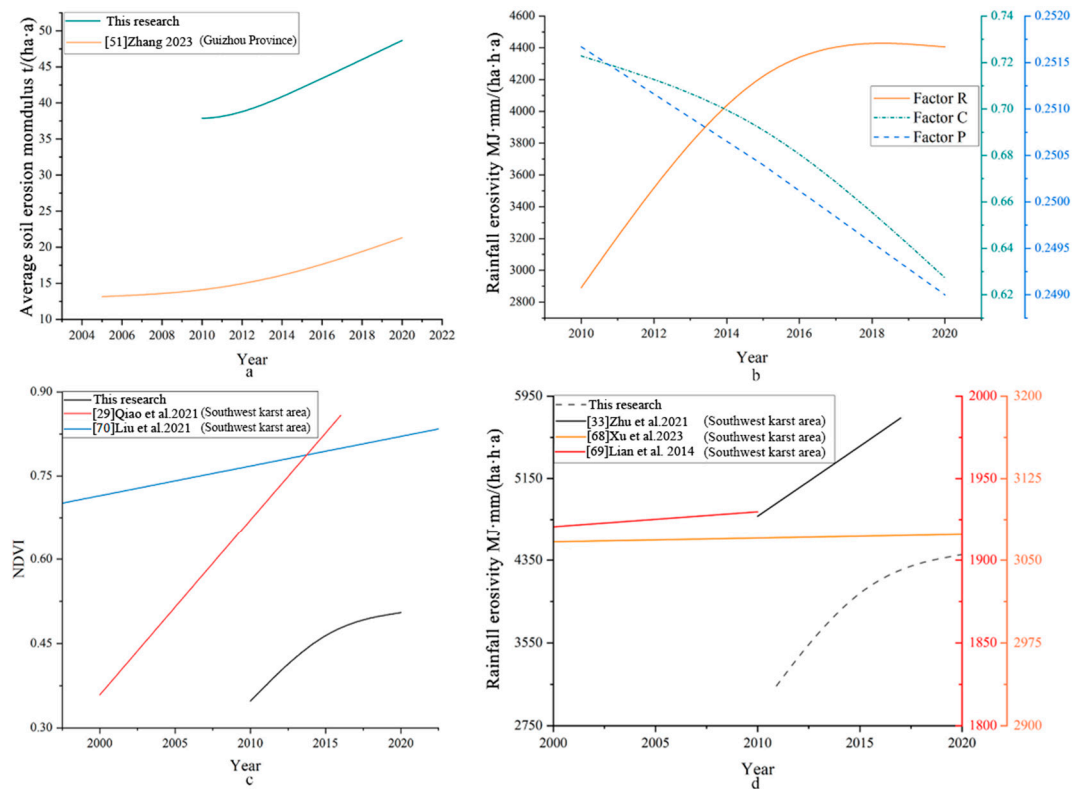


**Figure 16.** Trend plots ((a) shows the results of this study compared with other studies; (b) shows the trend of the factors in this study; (c) shows the results of the NDVI in this study compared with other studies; and (d) shows the results of the factor R in this study compared with other studies) [29,33,51,68–70].

#### 4.4. Type of Soil Erosion

The occurrence of soil erosion is the result of a complex interaction between human activities and natural factors [71]. The combined contribution rate of anthropogenic and natural soil erosion reflects the influence of human and natural processes on soil erosion. From 2015 to 2020, the area of AGH in the eastern part of the Karst plateau area exhibited a gradual increase, while the western part remained almost unchanged. Jiang et al. [48] demonstrated that elevation exerts a significant influence on human activities and rainfall patterns. They observed that rainfall tends to increase when the air is cooled by elevation, and subsequently declines when water vapor is depleted. This phenomenon has been corroborated by Zhang [51]. In the short term, human activities primarily impact vegetation and land use types, which only influence soil erosion to a limited extent. These activities are not the primary drivers of soil erosion. Rainfall is the primary source of soil erosion power. The lower erosive power of rainfall in the western part of the Karst plateau in southwest China results in a reduced or amplified effect of human activities on soil erosion in this area. The undulation of the land surface provides power conditions for slope flow, and the relatively flat terrain of Western and eastern parts of the Karst plateau in southwest China relies on the topography to weaken the erosion of soil by water flow, which also further weakens the “reduction/amplification effect” of human activities. From an anthropogenic perspective, studies [71] have demonstrated that human activities such as agriculture may contribute to soil erosion. However, soil erosion control has been conducted annually in the Karst plateau in southwest China. The high altitude of Weining, which also makes transport challenging, has resulted in a lack of local industry and minimal disturbance of the land by human activities. Consequently, despite the city of Weining having the highest population density and the largest agricultural sector, the soil erosion modulus has remained stable for an extended period.

In conclusion, the deterioration of soil erosion in the Karst plateau in southwest China is a consequence of climate change. Despite the implementation of numerous policies and projects to alleviate soil erosion, these have not been effective in halting the increasing trend of soil erosion. It is, therefore, imperative that soil and water conservation techniques be updated with alacrity to counteract the climatic context in which the erosive power of rainfall is increasing year by year. It is also worthy of note that the AGH area is still increasing, for example, in Jinsha County, even though overall human activities play a significant role in curbing soil erosion. While human activities have largely mitigated the adverse effects of soil erosion, in certain areas, human activities have exacerbated the problem due to the influence of natural factors and the interference of human activities of various kinds. This indicates that the incidence of heavy erosion, which is the focus of soil and water conservation measures, has been reduced. However, some of the erosion patterns close to the critical point are susceptible to deterioration due to the influence of human activities. This reflects the emphasis placed on treatment and a slight lack of prevention in previous soil and water conservation work. It is therefore worthy of attention in future soil and water conservation work.

#### 4.5. The Relationship Between Vegetation and Soil Erosion on Different Land Types

Sobol global sensitivity analysis is a common method of sensitivity analysis, which performs well in global sensitivity measurements [72]. In order to determine the effect of each factor on soil erosion, this study used the Python language Sobol global sensitivity analysis of each factor of the RUSLE model based on the SALib library. The first-order sensitivity index of the R factor is  $-0.0008$ , and the rest are around 0.1 (Table 7). The total sensitivity index is the same, except for R, which is 0.0423, and the other factors are around 0.3 (Table 7). The effect of the R factor on the soil erosion modulus is so small that it is negligible (this may be due to the small study area), while the sensitivities of the other factors are close to each other, which indicates that the settings of the factors in the RUSLE model are relatively reasonable. The total sensitivity index of Rock is the largest, which also reflects that bedrock exposure is a non-negligible part of the soil erosion process in the karst region; as a karst plateau region, the topography of Bijie City has great ups and downs, so the LS factor has a significant effect on the soil erosion. As a karst plateau area, the topography of Bijie City has great ups and downs, so the LS factor has the second highest total sensitivity index.

**Table 7.** Sensitivity analysis.

Factor	First-Order Sensitivity Index	Total Sensitivity Index
R	$-0.0008$	0.0423
K	0.0987	0.3064
LS	0.1041	0.3334
C	0.0984	0.3009
P	0.0754	0.2935
ROCK	0.1056	0.3445

In addition, the Sobol sensitivity analysis supports the analysis of the interaction between factors (Figure 17). C and P, the two factors dominated by human activities, have the largest effect on soil erosion after interaction (0.0504), but all the sensitivities of the factors in the figure are less than 0.06, which means that the effect of the interaction between the two factors on soil erosion is relatively small.

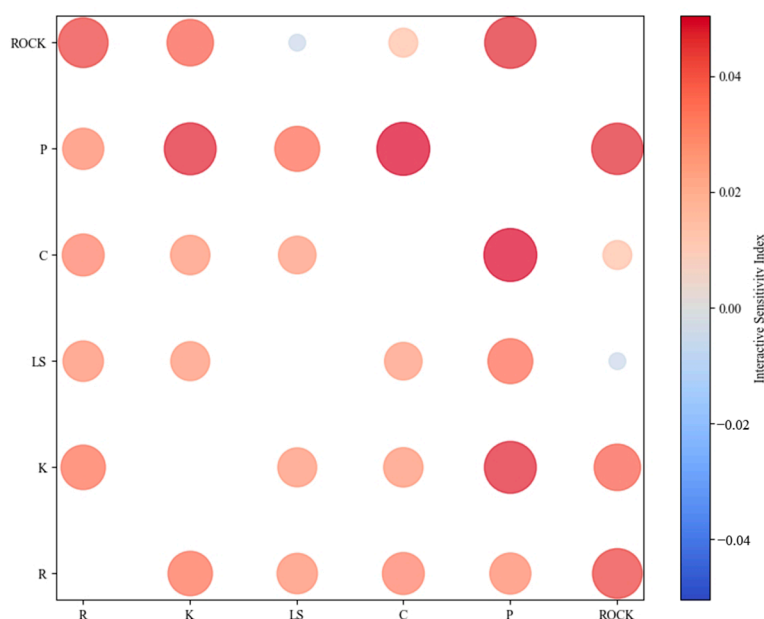
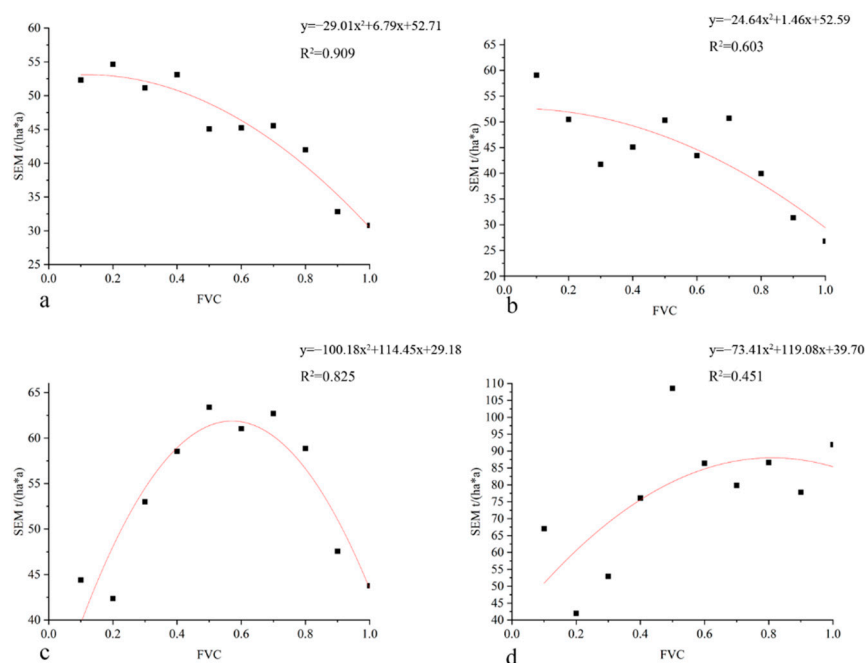


Figure 17. Interactive sensitivity index.

Increasing vegetation cover has a good mitigating effect on soil erosion [73,74]. To further discuss the relationship between vegetation restoration and soil erosion in karst areas, we analyzed the relationship between soil erosion and vegetation cover of four land types. As shown in Figure 18, the soil erosion modulus gradually decreased with the increase in vegetation cover in forests, especially as the decrease in the soil erosion modulus was accelerated after the vegetation cover exceeded 30%. Fonseca et al. (2023) found that, with the restoration of vegetation cover from 0% to 65%, the soil erosion modulus of the restored vegetation area decreased to 2% of that of bare land in the karst savanna area [75]. Liang et al. (2023) investigated the soil physicochemical properties of three artificial restoration measures in arbor forest, orchard, grassland, and farmland (control), which were continuously implemented for 16 years, and the results showed that the soil bulk density decreased, the capillary porosity increased, the soil water stable aggregates increased, and the soil erodibility decreased by about 15% after vegetation restoration [76]. Jiang et al. (2009) pointed out that, in the karst region, soil erosion is greatly reduced when the vegetation cover exceeds 60%, while soil loss is large when the vegetation cover is less than 20% [77]. For “binary” erosion in karst areas, vegetation restoration can also significantly improve the soil erosion resistance in the 10–20 cm soil layer in the fissure zone [78]. It is clear that afforestation has an excellent effect on soil erosion, so we suggest that afforestation should be carried out with a vegetation cover of more than 30%, preferably up to 60%.

There is a parabolic relationship between the soil erosion modulus and vegetation cover in cropland, with the highest soil erosion modulus at 60% vegetation cover. In Bijie, farmland abandonment is a common phenomenon, Liu and Han (2020) showed that the SOC of farmland after abandonment was close to that of the native vegetation area and significantly higher than that of farmland [79]; and Yan et al. (2023) found that the physicochemical properties of soils in karst areas deteriorated and then improved after farmland abandonment, which helped to increase the resistance of soils to erosion. This is the reason why the soil erosion modulus is lower when the vegetation cover is low [78]. Furthermore, the vegetation cover of arable land is a dynamic process involving a sowing phase, a crop growing phase, and a crop harvesting phase. Predictably, vegetation cover is low at the beginning and end of the ploughing period and is often accompanied by soil turning, a series of actions that can weaken the soil’s ability to resist erosion, resulting in an increase in soil erosion. During the growth phase of the crop, the vegetation cover is

higher, the leaves reduce the kinetic energy of the raindrops, and the root system increases the soil's resistance to erosion, resulting in a lower soil erosion modulus. In response to this phenomenon, it is recommended that soil erosion protection be provided in the early stages of cultivation, for example, by laying plastic sheeting over the exposed part of the soil.



**Figure 18.** Relationship between soil erosion and vegetation coverage under different land types. (Note: (a) reflects the soil erosion of forest in different FVC; (b) reflects the soil erosion of grassland in different FVC; (c) reflects the soil erosion of cultivated land in different FVC. (d) reflects soil erosion of shrubs in different FVC).

Grasslands are similar to forests in that there is a negative correlation between vegetation cover and soil erosion. However, in scrubland, there is a positive correlation between vegetation cover and soil erosion, and, when the vegetation cover of scrubland reaches 60%, the soil erosion modulus reaches the highest and gradually stabilizes, which is completely different from other land types. Shrubs and herbaceous plants grow in similar environments and there is a competitive relationship between them, and an increase in shrubs means a decrease in herbaceous plants [80]. Soils with herbaceous vegetation have a higher shear strength and aggregate stability than planted shrubs and trees [81]. Leite et al. (2020) also showed that sand production in areas with high herbaceous vegetation cover was significantly higher than that in areas with high shrub vegetation cover [82]. An increase in shrub cover can lead to bare surface soil and the loosening of the soil, resulting in increased soil erosion [80]. Therefore, we believe that future soil and water conservation efforts should address the damage to soil erosion resistance caused by shrub encroachment. In native grassland areas, shrubs should be prevented from encroaching on the habitat of herbaceous vegetation; in scrub areas, shrub and grass structures need to be optimized to a reasonable degree to prevent soil erosion.

#### 4.6. Deficiencies and Prospects

As shown in Figure 3, we find in the accuracy verification process that Dingjiazhai's predicted value is far lower than the measured value. In order to improve the accuracy, we added the rock exposure to the RUSLE model to consider the complex soil erosion in the karst plateau region. However, it is undeniable that the natural environment of the karst region is extremely complex with high terrain fragmentation. Zeng et al. (2018) classified the soil erosion in the karst region of southwest China into three types, SA, SB, and SC,

through field surveys [83]; Fan et al. (2023) classified the soil erosion of karst slopes into three types, RES, RCS, and SCR, based on the rock exposure from the microscopic point of view [84]; and Fan et al. (2023) classified the soil erosion of karst slopes into three types, RES, RCS and SCR, based on the rock exposure from the microscopic point of view [85]. RES, RCS, and SCR categories [84]. In addition, as shown in Figure 13, factors such as the altitude, slope, vegetation type, and population density affect soil erosion in the study area. It can be seen that the soil erosion modulus in karst areas is caused by many factors, especially in the regional scale study of karst plateau areas. The same vegetation cover and the same vegetation type may produce very different soil erosion situations when they are encountered in different geographical strips. Feng et al. (2020) found a similar situation and pointed out that factors such as the sustainability of vegetation cover, drought, and rock type may affect the effect of vegetation restoration on the control of soil erosion in karst regions [85]. Therefore, we believe it is necessary to pay attention to this point in future research on soil erosion in karst areas.

## 5. Conclusions

In this study, the QAM model is improved based on the RUSLE model. The objective is to evaluate soil erosion in the Karst plateau, including anthropogenic and natural soil erosion, and to determine the soil erosion types in the study area. The results of the study are presented below:

- (1) The SEM in the study area increased year by year from 2010 to 2020, and the rate of increase was accelerating. The average erosion modulus rose by 11% in 2015 compared to 2010, and by 16% in 2020 compared to 2015;
- (2) The anthropogenic soil erosion modulus in the study area was  $-13.79$ , and  $-17.36$  t/(ha·a) in 2015 and 2020, respectively, indicating that human activities have reduced soil erosion in general;
- (3) The type of study area is characterized by a dominance of natural factors (AGN) in soil erosion, with a proportion of human-induced factors (AGH) increasing.

This study addresses a gap in the quantitative study of anthropogenic soil erosion in the Karst plateau area by analyzing the role of natural factors and human activities on soil erosion in the Bijie area in terms of mechanism. Furthermore, this study expands the scope of the application of the QAM and provides a new way of thinking for theoretical research in this field.

**Author Contributions:** Conceptualization, X.G.; data curation, X.G.; formal analysis, Z.Z. and J.Z.; funding acquisition, P.Y.; investigation, J.Z.; project administration, P.Y.; resources, P.Y.; software, Z.Z.; supervision, J.Z.; visualization, X.G. and C.Y.; writing—original draft, X.G.; writing—review and editing, P.Y. All authors have read and agreed to the published version of the manuscript.

**Funding:** This study is financially supported by the National Natural Science Foundation of China (32101593); the Natural Science Foundation of Guizhou Province (Qiankehe Jichu-ZK [2021]220); the Guizhou Normal University Academic New Seedling Fund Project (Qian Shi Xin Miao [2022] 09); and the Guizhou Normal University Academic New Seedling Fund Project (Qian Shi Xin Miao [2022]23).

**Data Availability Statement:** All data sources are described in the manuscript.

**Conflicts of Interest:** The authors declare no conflicts of interest.

## References

1. Pimentel, D. Soil Erosion: A Food and Environmental Threat. *Environ. Dev. Sustain.* **2006**, *8*, 119–137. [[CrossRef](#)]
2. Zuazo, V.H.D.; Pleguezuelo, C.R.R. *Soil-Erosion and Runoff Prevention by Plant Covers: A Review*; Springer eBooks: New York, NY, USA, 2009; pp. 785–811. [[CrossRef](#)]
3. Lang, Y.; Yang, X.; Cai, H. Quantifying anthropogenic soil erosion at a regional scale—The case of Jiangxi Province, China. *CATENA* **2023**, *226*, 107081. [[CrossRef](#)]
4. Lal, R. Soil Erosion and Gaseous Emissions. *Appl. Sci.* **2020**, *10*, 2784. [[CrossRef](#)]
5. Jin, F.; Yang, W.; Fu, J.; Li, Z. Effects of vegetation and climate on the changes of soil erosion in the Loess Plateau of China. *Sci. Total Environ.* **2021**, *773*, 145514. [[CrossRef](#)]

6. Ma, X.; Zhao, C.; Zhu, J. Aggravated risk of soil erosion with global warming—A global meta-analysis. *CATENA* **2021**, *200*, 105129. [[CrossRef](#)]
7. Zhang, C.; Zhou, A.; Zhang, H.; Zhang, Q.; Zhang, X.; Sun, H.; Zhao, C. Soil erosion in relation to climate change and vegetation cover over the past 2000 years as inferred from the Tianchi lake in the Chinese Loess Plateau. *J. Asian Earth Sci.* **2019**, *180*, 103850. [[CrossRef](#)]
8. Wang, L.; Zhang, F.; Fu, S.; Shi, X.; Chen, Y.; Jagirani, M.D.; Zeng, C. Assessment of soil erosion risk and its response to climate change in the mid-Yarlung Tsangpo River region. *Environ. Sci. Pollut. Res. Int.* **2019**, *27*, 607–621. [[CrossRef](#)] [[PubMed](#)]
9. Liu, Y.; Fu, B.; Lü, Y.; Wang, Z.; Gao, G. Hydrological responses and soil erosion potential of abandoned cropland in the Loess Plateau, China. *Geomorphology* **2012**, *138*, 404–414. [[CrossRef](#)]
10. Nearing, M.A.; Jetten, V.; Baffaut, C.; Cerdan, O.; Couturier, A.; Hernandez, M.; Bissonnais, Y.L.; Nichols, M.H.; Nunes, J.P.; Renschler, C.S.; et al. Modeling response of soil erosion and runoff to changes in precipitation and cover. *CATENA* **2005**, *61*, 131–154. [[CrossRef](#)]
11. Bodí, M.B.; Doerr, S.H.; Cerdà, A.; Mataix-Solera, J. Hydrological effects of a layer of vegetation ash on underlying wettable and water-repellent soil. *Geoderma* **2012**, *191*, 14–23. [[CrossRef](#)]
12. Zhou, J.; Fu, B.; Gao, G.; Lü, Y.; Liu, Y.; Lü, N.; Wang, S. Effects of precipitation and restoration vegetation on soil erosion in a semi-arid environment in the Loess Plateau, China. *CATENA* **2016**, *137*, 1–11. [[CrossRef](#)]
13. Wang, H.; Zhao, W.; Li, C.; Pereira, P. Vegetation greening partly offsets the water erosion risk in China from 1999 to 2018. *Geoderma* **2021**, *401*, 115319. [[CrossRef](#)]
14. Zhang, X.; Song, J.; Wang, Y.; Sun, H.; Li, Q. Threshold effects of vegetation coverage on runoff and soil loss in the Loess Plateau of China: A meta-analysis. *Geoderma* **2022**, *412*, 115720. [[CrossRef](#)]
15. Diatta, A.A.; Thomason, W.E.; Abaye, O.; Thompson, T.L.; Battaglia, M.L.; Vaughan, L.J.; Lo, M.; Filho, J.F.D.C.L. Assessment of Nitrogen Fixation by Mungbean Genotypes in Different Soil Textures Using <sup>15</sup>N Natural Abundance Method. *J. Soil Sci. Plant Nutr.* **2020**, *20*, 2230–2240. [[CrossRef](#)]
16. Spurgeon, D.J.; Keith, A.M.; Schmidt, O.; Lammertsma, D.R.; Faber, J.H. Land-use and land-management change: Relationships with earthworm and fungi communities and soil structural properties. *BMC Ecol.* **2013**, *13*, 46. [[CrossRef](#)]
17. Adeyemi, O.; Keshavarz-Afshar, R.; Jahanzad, E.; Battaglia, M.L.; Luo, Y.; Sadeghpour, A. Effect of Wheat Cover Crop and Split Nitrogen Application on Corn Yield and Nitrogen Use Efficiency. *Agronomy* **2020**, *10*, 1081. [[CrossRef](#)]
18. Babur, E.; Uslu, M.S.; Battaglia, M.L.; Diatta, A.; Fahad, S.; Datta, R.; Zafar-Ul-Hye, M.; Hussain, G.S.; Danish, S. Studying soil erosion by evaluating changes in physico-chemical properties of soils under different land-use types. *J. Saudi Soc. Agric. Sci.* **2021**, *20*, 190–197. [[CrossRef](#)]
19. Gocić, M.; Dragičević, S.; Radivojević, A.; Bursać, N.M.; Stričević, L.; Đorđević, M. Changes in Soil Erosion Intensity Caused by Land Use and Demographic Changes in the Jablanica River Basin, Serbia. *Agriculture* **2020**, *10*, 345. [[CrossRef](#)]
20. Zhao, J.; Wang, Z.; Dong, Y.; Yang, Z.; Govers, G. How soil erosion and runoff are related to land use, topography and annual precipitation: Insights from a meta-analysis of erosion plots in China. *Sci. Total Environ.* **2022**, *802*, 149665. [[CrossRef](#)]
21. Obiahu, O.H.; Elias, E. Effect of land use land cover changes on the rate of soil erosion in the Upper Eyiohia river catchment of Afikpo North Area, Nigeria. *Environ. Chall.* **2020**, *1*, 100002. [[CrossRef](#)]
22. Borrelli, P.; Robinson, D.A.; Fleischer, L.R.; Lugato, E.; Ballabio, C.; Alewell, C.; Meusburger, K.; Modugno, S.; Schütt, B.; Ferro, V.; et al. An assessment of the global impact of 21st century land use change on soil erosion. *Nat. Commun.* **2017**, *8*, 2013. [[CrossRef](#)]
23. Zhen, L. The national census for soil erosion and dynamic analysis in China. *Int. Soil Water Conserv. Res.* **2013**, *1*, 12–18. [[CrossRef](#)]
24. Han, X.; Lv, P.; Zhao, S.; Sun, Y.; Yan, S.; Wang, M.; Han, X.; Wang, X. The Effect of the Gully Land Consolidation Project on Soil Erosion and Crop Production on a Typical Watershed in the Loess Plateau. *Land* **2018**, *7*, 113. [[CrossRef](#)]
25. Han, Z.; Yang, X.; Yin, X.; Fang, Q.; Zhao, L. How do the distribution patterns of exposed roots affect the rainfall-runoff processes of sloped land under simulated multi-rainfall conditions in karst region? *CATENA* **2024**, *236*, 107708. [[CrossRef](#)]
26. Wang, L.C.; Lee, D.W.; Zuo, P.; Zhou, Y.K.; Xu, Y.P. Karst environment and eco-poverty in southwestern China: A case study of Guizhou Province. *Chin. Geogr. Sci.* **2004**, *14*, 21–27. [[CrossRef](#)]
27. Yang, R.; Zhong, C.; Yang, Z.; Liu, F.; Peng, H. Analysis on poverty influencing factors in deep poverty county of Karst Rocky-desertified Area in Southwest China. *World Geogr. Res.* **2022**, *31*, 1298–1309. [[CrossRef](#)]
28. Zhang, J.Y.; Dai, M.H.; Wang, L.C.; Zeng, C.F.; Su, W.C. The challenge and future of rocky desertification control in karst areas in southwest China. *Solid Earth* **2016**, *7*, 83–91. [[CrossRef](#)]
29. Qiao, Y.; Jiang, Y.; Zhang, C. Contribution of karst ecological restoration engineering to vegetation greening in southwest China during recent decade. *Ecol. Indic.* **2021**, *121*, 107081. [[CrossRef](#)]
30. Tong, X.; Brandt, M.; Yue, Y.; Horion, S.; Wang, K.; De Keersmaecker, W.; Tian, F.; Schurgers, G.; Xiao, X.; Luo, Y.; et al. Increased vegetation growth and carbon stock in China karst via ecological engineering. *Nat. Sustain.* **2018**, *1*, 44–50. [[CrossRef](#)]
31. Yang, F.; Lu, C. Spatiotemporal variation and trends in rainfall erosivity in China's dryland region during 1961–2012. *CATENA* **2015**, *133*, 362–372. [[CrossRef](#)]
32. Peng, J.; Tian, L.; Zhang, Z.; Zhao, Y.; Green, S.M.; Quine, T.A.; Liu, H.; Meersmans, J. Distinguishing the impacts of land use and climate change on ecosystem services in a karst landscape in China. *Ecosyst. Serv.* **2020**, *46*, 101199. [[CrossRef](#)]
33. Zhu, D.; Xiong, K.; Xiao, H. Multi-time scale variability of rainfall erosivity and erosivity density in the karst region of southern China, 1960–2017. *CATENA* **2021**, *197*, 104977. [[CrossRef](#)]

34. Shi, J. Evaluation and countermeasure analysis of comprehensive control of stony desertification in Bijie City. Master's Thesis, Guizhou University, Guiyang, China, 2021. (In Chinese).
35. Pan, L.D.; Li, R.; Shu, D.C.; Zhao, L.N.; Chen, M.; Jing, J. Effects of rainfall and rocky desertification on soil erosion in karst area of Southwest China. *J. Mt. Sci.* **2022**, *19*, 3118–3130. [[CrossRef](#)]
36. Yu, B.; Rosewell, C. An assessment of a daily rainfall erosivity model for New South Wales. *Soil Res.* **1996**, *34*, 139. [[CrossRef](#)]
37. Sharpley, A.; Williams, J.R. *EPIC-Erosion/Productivity Impact Calculator: 1. Model Documentation*; US Government Printing Office: Washington, DC, USA, 1990.
38. Cai, C.; Ding, S.; Shi, H.; Huang, L.; Zhang, G. Prediction of soil erosion in a small watershed using USLE model and IDRISI. *J. Soil Water Conserv.* **2000**, *2*, 19–24. (In Chinese)
39. McCool, N.D.K.; Brown, N.L.C.; Foster, N.G.R.; Mutchler, N.C.K.; Meyer, N.L.D. Revised Slope Steepness Factor for the Universal Soil Loss Equation. *Trans. ASAE* **1987**, *30*, 1387–1396. [[CrossRef](#)]
40. McCool, N.D.K.; Foster, N.G.R.; Mutchler, N.C.K.; Meyer, N.L.D. Revised Slope Length Factor for the Universal Soil Loss Equation. *Trans. ASAE* **1989**, *32*, 1571–1576. [[CrossRef](#)]
41. Ghosal, K.; Bhattacharya, S.D. A Review of RUSLE Model. *Photonirvachak* **2020**, *48*, 689–707. [[CrossRef](#)]
42. Rao, W.; Shen, Z.; Duan, X. Spatiotemporal patterns and drivers of soil erosion in Yunnan, Southwest China: RUSLE assessments for recent 30 years and future predictions based on CMIP6. *CATENA* **2023**, *220*, 106703. [[CrossRef](#)]
43. Getachew, B.; Manjunatha, B.R.; Bhat, G.H. Assessing current and projected soil loss under changing land use and climate using RUSLE with Remote sensing and GIS in the Lake Tana Basin, Upper Blue Nile River Basin, Ethiopia. *Egypt. J. Remote Sens. Space Sci.* **2021**, *24*, 907–918. [[CrossRef](#)]
44. Wu, Y.; Yang, J.; Li, S.; Guo, C.; Yang, X.; Xu, Y.; Yue, F.; Peng, H.; Chen, Y.; Gu, L.; et al. NDVI-Based Vegetation Dynamics and Their Responses to Climate Change and Human Activities from 2000 to 2020 in Miaoling Karst Mountain Area, SW China. *Land* **2023**, *12*, 1267. [[CrossRef](#)]
45. Yang, Q. Study on the Contribution Rate of Soil Surface-Subsurface Loss and Its Influencing Factors in a Typical Areas of Karst Rocky Desertification in Plateau Mountains. Master's Thesis, Guizhou Normal University, Gui Yang, China, 2023. Available online: <https://link.cnki.net/doi/10.27048/d.cnki.ggzsu.2023.001274> (accessed on 27 September 2024). (In Chinese)
46. Guizhou Provincial Development and Reform Commission. The Ecological Construction of Guizhou Province Will Enter a Stage to Ensure the Harmonious Development of Man and Nature. Guizhou Provincial People's Government 2011, March 10. Available online: [https://www.guizhou.gov.cn/home/gzyw/202109/t20210913\\_70337228.html](https://www.guizhou.gov.cn/home/gzyw/202109/t20210913_70337228.html) (accessed on 1 September 2023).
47. Jain, S.K.; Goel, M.K. Assessing the vulnerability to soil erosion of the Ukai Dam catchments using remote sensing and GIS. *Hydrol. Sci. J.* **2002**, *47*, 31–40. [[CrossRef](#)]
48. Jiang, Y.; Gao, J.; Yang, L.; Wu, S.; Dai, E. The interactive effects of elevation, precipitation and lithology on karst rainfall and runoff erosivity. *CATENA* **2021**, *207*, 105588. [[CrossRef](#)]
49. Qu, K. Study on Evaluation of Geological Hazard Susceptibility of Collapse and Landslide in Bijie City, Guizhou Province. Master's Thesis, Jilin University, Changchun, China, 2020. Available online: <https://link.cnki.net/doi/10.27162/d.cnki.gjlin.2019.000616> (accessed on 27 September 2024). (In Chinese)
50. Huang, Z.; Yu, J.; Fang, L.; Fang, F.; Miao, Y.; Zhi, J.; Xu, G.; Shui, H.; Cao, Y. Study on soil erosion and its influencing factors in Qingyijiang River Basin based on InVEST model. *J. Soil Water Conserv.* **2023**, *37*, 189–197. (In Chinese)
51. Zhang, Y. Soil Erosion Patterns and Driving Mechanisms Based on the Degree of Karst Development. Master's Thesis, Guizhou Normal University, Gui Yang, China, 2023. Available online: <https://link.cnki.net/doi/10.27048/d.cnki.ggzsu.2023.001161> (accessed on 27 September 2024). (In Chinese)
52. Assouline, S.; Ben-Hur, M. Effects of rainfall intensity and slope gradient on the dynamics of interracial erosion during soil surface sealing. *CATENA* **2006**, *66*, 211–220. [[CrossRef](#)]
53. Devia, G.K.; Ganasri, B.; Dwarakish, G. A Review on Hydrological Models. *Aquat. Procedia* **2015**, *4*, 1001–1007. [[CrossRef](#)]
54. Wakiyama, Y.; Onda, Y.; Mizugaki, S.; Asai, H.; Hiramatsu, S. Soil erosion rates on forested mountain hillslopes estimated using <sup>137</sup>Cs and <sup>210</sup>Pbex. *Geoderma* **2010**, *159*, 39–52. [[CrossRef](#)]
55. Juan, J.; Dongdong, L.; YuanHang, F.; Pu, L. Combined effects of moss colonization and rock fragment coverage on sediment losses, flow hydraulics and surface microtopography of carbonate-derived laterite from karst mountainous lands. *CATENA* **2023**, *229*, 107202. [[CrossRef](#)]
56. Mushi, C.; Ndomba, P.; Trigg, M.; Tshimanga, R.; Mtalo, F. Assessment of basin-scale soil erosion within the Congo River Basin: A review. *CATENA* **2019**, *178*, 64–76. [[CrossRef](#)]
57. Wen, X.; Deng, X. Current soil erosion assessment in the Loess Plateau of China: A mini-review. *J. Clean. Prod.* **2020**, *276*, 123091. [[CrossRef](#)]
58. Li, Y.; Bai, X.; Zhou, Y.; Qin, L.; Tian, X.; Tian, Y.; Li, P. Spatial–Temporal Evolution of Soil Erosion in a Typical Mountainous Karst Basin in SW China, Based on GIS and RUSLE. *Arab. J. Sci. Eng. Sect. B Eng.* **2015**, *41*, 209–221. [[CrossRef](#)]
59. Yang, X.; Sun, W.; Li, P.; Mu, X.; Gao, P.; Zhao, G. Reduced sediment transport in the Chinese Loess Plateau due to climate change and human activities. *Sci. Total Environ.* **2018**, *642*, 591–600. [[CrossRef](#)] [[PubMed](#)]
60. Zhang, G.; Shen, R.; Luo, R.; Cao, Y.; Zhang, X. Effects of sediment load on hydraulics of overland flow on steep slopes. *Earth Surf. Process. Landf.* **2010**, *35*, 1811–1819. [[CrossRef](#)]

61. Wang, H.; Gao, J.; Hou, W. Quantitative attribution analysis of soil erosion in different geomorphological types in karst areas: Based on the geodetector method. *J. Geogr. Sci.* **2019**, *29*, 271–286. [[CrossRef](#)]
62. Santhanam, H.; Majumdar, R. Quantification of green-blue ratios, impervious surface area and pace of urbanisation for sustainable management of urban lake—Land zones in India—A case study from Bengaluru city. *J. Urban Manag.* **2022**, *11*, 310–320. [[CrossRef](#)]
63. Li, R.; Wu, Q.; Zhang, J.; Wen, Y.; Li, Q. Effects of Land Use Change of Sloping Farmland on Characteristic of Soil Erosion Resistance in Typical Karst Mountainous Areas of Southwestern China. *Pol. J. Environ. Stud.* **2019**, *28*, 2707–2716. [[CrossRef](#)]
64. Niu, L.; Shao, Q. Soil Conservation Service Spatiotemporal Variability and Its Driving Mechanism on the Guizhou Plateau, China. *Remote Sens.* **2020**, *12*, 2187. [[CrossRef](#)]
65. Chen, M.; Gao, J.Y.; Chen, H.L.; Jing, J.; Li, R. Elevation, bedrock exposure, land use, interbedded limestone and clastic rock, and vegetation coverage dominate the spatiotemporal variability of soil erosion in karst basin. *J. Mt. Sci.* **2023**, *20*, 2519–2535. [[CrossRef](#)]
66. Ma, Y.; Zuo, L.; Gao, J.; Liu, Q.; Liu, L. The karst NDVI correlation with climate and its BAS-BP prediction based on multiple factors. *Ecol. Indic.* **2021**, *132*, 108254. [[CrossRef](#)]
67. Xu, Y.; Dai, Q.Y.; Lu, Y.G.; Zhao, C.; Huang, W.T.; Xu, M.; Feng, Y.X. Identification of ecologically sensitive zones affected by climate change and anthropogenic activities in Southwest China through a NDVI-based spatial-temporal model. *Ecol. Indic.* **2024**, *158*, 111482. [[CrossRef](#)]
68. Xu, X.; Yan, Y.; Dai, Q.; Yi, X.; Hu, Z.; Cen, L. Spatial and temporal dynamics of rainfall erosivity in the karst region of southwest China: Interannual and seasonal changes. *CATENA* **2023**, *221*, 106763. [[CrossRef](#)]
69. Lian, Y.; You, G.J.Y.; Lin, K.; Jiang, Z.; Zhang, C.; Qin, X. Characteristics of climate change in southwest China karst region and their potential environmental impacts. *Environ. Earth Sci.* **2014**, *74*, 937–944. [[CrossRef](#)]
70. Liu, Z.; Zhang, Y. Vegetation cover change and its response to human activities in the southwestern karst region of China. *Front. Ecol. Evol.* **2024**, *12*, 1326601. [[CrossRef](#)]
71. He, X.; Zhou, J.; Zhang, X.; Tang, K. Soil erosion response to climatic change and human activity during the Quaternary on the Loess Plateau, China. *Reg. Environ. Change* **2006**, *6*, 62–70. [[CrossRef](#)]
72. Sysoev, A. Sensitivity Analysis of Mathematical Models. *Computation* **2023**, *11*, 159. [[CrossRef](#)]
73. Ouyang, W.; Hao, F.; Skidmore, A.K.; Toxopeus, A. Soil erosion and sediment yield and their relationships with vegetation cover in upper stream of the Yellow River. *Sci. Total Environ.* **2010**, *409*, 396–403. [[CrossRef](#)] [[PubMed](#)]
74. Xu, J.; Zhang, Y.; Huang, C.; Zeng, L.; Teng, M.; Wang, P.; Xiao, W. Forest restoration shows uneven impacts on soil erosion, net primary productivity and livelihoods of local households. *Ecol. Indic.* **2021**, *134*, 108462. [[CrossRef](#)]
75. Fonseca, M.R.S.; Uagoda, R.E.S.; Chaves, H.M.L. Runoff, soil loss, and water balance in a restored Karst area of the Brazilian Savanna. *CATENA* **2022**, *222*, 106878. [[CrossRef](#)]
76. Liang, P.; Wang, X.; Xu, Q.; Zhang, J.; Fang, R.; Fu, Z.; Chen, H. Lithology-mediated soil erodibility characteristics after vegetation restoration in the karst region of Southwest China. *Land Degrad. Dev.* **2023**, *35*, 1070–1086. [[CrossRef](#)]
77. Jiang, Y.; Li, L.; Groves, C.; Yuan, D.; Kambesis, P. Relationships between rocky desertification and spatial pattern of land use in typical karst area, Southwest China. *Environ. Earth Sci.* **2009**, *59*, 881–890. [[CrossRef](#)]
78. Yan, Y.; Dai, Q.; Yang, Y.; Lan, X. Effects of vegetation restoration types on soil erosion reduction of a shallow karst fissure soil system in the degraded karst areas of Southwestern China. *Land Degrad. Dev.* **2023**, *34*, 2241–2255. [[CrossRef](#)]
79. Liu, M.; Han, G. Assessing soil degradation under land-use change: Insight from soil erosion and soil aggregate stability in a small karst catchment in southwest China. *PeerJ* **2020**, *8*, e8908. [[CrossRef](#)] [[PubMed](#)]
80. Liu, Y.; Fang, H.; Huang, Z.; Leite, P.A.; Liu, Y.; López-Vicente, M.; Zhao, J.; Shi, Z.; Wu, G. Shrub encroachment increases soil erosion risk in hillside alpine meadows of the Qinghai-Tibetan Plateau, NW China. *CATENA* **2022**, *222*, 106842. [[CrossRef](#)]
81. Fattet, M.; Fu, Y.; Ghestem, M.; Ma, W.; Foulonneau, M.; Nespoulous, J.; Bissonnais, Y.L.; Stokes, A. Effects of vegetation type on soil resistance to erosion: Relationship between aggregate stability and shear strength. *CATENA* **2011**, *87*, 60–69. [[CrossRef](#)]
82. Leite, P.A.M.; Wilcox, B.P.; McInnes, K.J. Woody plant encroachment enhances soil infiltrability of a semiarid karst savanna. *Environ. Res. Commun.* **2020**, *2*, 115005. [[CrossRef](#)]
83. Zeng, F.; Jiang, Z.; Shen, L.; Chen, W.; Yang, Q.; Zhang, C. Assessment of multiple and interacting modes of soil loss in the karst critical zone, Southwest China (SWC). *Geomorphology* **2018**, *322*, 97–106. [[CrossRef](#)]
84. Fan, C.; Zhao, L.; Hou, R.; Fang, Q.; Zhang, J. Quantitative analysis of rainwater redistribution and soil loss at the surface and belowground on karst slopes at the microplot scale. *CATENA* **2023**, *227*, 107113. [[CrossRef](#)]
85. Feng, S.; Wu, L.; Liang, B.; Wang, H.; Liu, H.; Zhu, C.; Li, S. Forestation does not necessarily reduce soil erosion in a karst watershed in southwestern China. *Prog. Phys. Geogr. Earth Environ.* **2020**, *45*, 82–97. [[CrossRef](#)]

**Disclaimer/Publisher’s Note:** The statements, opinions and data contained in all publications are solely those of the individual author(s) and contributor(s) and not of MDPI and/or the editor(s). MDPI and/or the editor(s) disclaim responsibility for any injury to people or property resulting from any ideas, methods, instructions or products referred to in the content.